mater.scichina.com link.springer.com

Published online 28 November 2023 | https://doi.org/10.1007/s40843-023-2678-5
Sci China Mater 2023, 66(12): 4521–4541

Ultimate structures in catalysis: Single atoms, subnano-clusters, and electrons

Honglin Wang[1], Jing Li[2] and Hongwei Zhu[1*]

ABSTRACT When reduced to the atomic level, catalysts exhibit greatly improved performance, i.e., improved atomic utilization, heightened coordination unsaturation, and increased specific surface area. Meticulous design concerning atomic distribution and electron behavior is vital for improving catalytic efficiency, introducing the concept of "ultimate structure" in catalysis. These structures span a broad range from single atoms (SAs) to dual atoms, single-atom chains/layers, and subnano-clusters (SNCs). By examining catalysts at the atomic and electronic levels using these ultimate structures, we can gain a deep understanding of their inherent properties and new directions for future catalytic design. This review delves into the recent progress and research directions of ultimate structures in catalysis, focusing on SAs, SNCs, and electron-level dynamics. In particular, we focus on advanced strategies such as metal-support bond enhancement, defect manipulation, and electron configuration control to optimize these ultimate structures. We also explore the interrelationships between various ultimate structures, underlining their unique attributes. This review outlines potential trajectories for the evolution of these catalysts with ultimate structures.

Keywords: ultimate structures, catalysts, single atoms, subnanoclusters

INTRODUCTION

The downsizing of catalysts has yielded remarkable improvements in catalysis [1,2]. As material size decreases, specific surface area, electronic structures, and quantum size effects significantly increase, prompting extensive exploration and manipulation of catalysts from a microscopic perspective [3–5]. Amid the pursuit of minimizing material dimensions, new catalysts transcending the conventional classification have proliferated in various reactions. The concept of single-atom catalysts (SACs) was initially introduced in 2011 to delineate catalysts with single atoms (SAs) anchored to support materials [6]. The first practically prepared SAC with Pt SAs on iron oxide nanocrystallites has a distinctive electronic structure capable of fine-tuning reaction pathways, demonstrating exceptional activity and selectivity. Since then, research on SACs considerably increased, inspiring enthusiasm toward diverse and well-designed microstructures in catalysis. Notable paradigms in the microstructures of catalysts include single-metal-atom chains (SMACs) and single-atom layers (SALs); these have exhibited considerable promise in catalysis [7–9]. Increasing studies of SAs lead to the further development of subnanoclusters (SNCs), comprising dual atoms to dozens of atoms with the size less than 2 nm [10]. Previous reports have revealed their compelling merits derived from size reduction and synergistic effects [11,12]. Moreover, the role of electrons as the smallest "structure" to modulate catalytic performance has attracted considerable attention [13,14]. Given the multifaceted improvements accomplished through dimension reduction, a comprehensive understanding of these structures in catalysis is required.

This review introduces "ultimate structure" as a paradigm of basic components to modulate catalytic performance, providing new insights into the evolving trend of size reduction in catalysis. The ultimate structures in catalysis are microstructures downsized to atomic and electronic levels, which are fundamental constituents of materials. Specifically, ultimate structures in catalysis are expounded upon the scale of SAs, SNCs, and electrons (Fig. 1). Studies of these dimensions manifest the trend of decreasing mass and increasing active sites for catalysts with ultimate structures, as well as reveal cross-dimensional interactions. Recent advancements and prevailing research trends on ultimate structures in catalysis are comprehensively analyzed in each category. Their catalytic performance in oxygen evolution reaction (OER), hydrogen evolution reaction (HER), carbon dioxide reduction reaction (CO_2RR), oxygen reduction reaction (ORR), nitrogen reduction reaction (N_2RR), and other electrochemical reactions, as well as the modulating strategies in metal–support interaction (MSI), defect engineering, and electronic structure, are discussed in detail. Finally, several perspective directions for the future development of ultimate structures in catalysis are proposed.

ULTIMATE STRUCTURE I: SAs

In recent research on catalysts, the significance of SAs has been increasingly recognized. The SACs are renowned for their maximized atomic utilization efficiency, which is attributed to the individually dispersed atoms on supports [3]. Beyond SACs, the significance of SAs in SMACs and SALs, which represents extensions of SACs with precisely arranged SAs, is also determined [8,15]. The common thread linking these kinds of catalysts is the composition of their active sites by one or several SAs, indicating that strategies aimed at modulating their catalytic performance should focus on the behavior of SAs. The

[1] State Key Lab of New Ceramics and Fine Processing, School of Materials Science and Engineering, Tsinghua University, Beijing 100084, China
[2] State Key Lab of Solid Waste Reuse for Building Materials, Beijing Building Materials Academy of Science Research, Beijing 100041, China
* Corresponding author (email: hongweizhu@tsinghua.edu.cn)

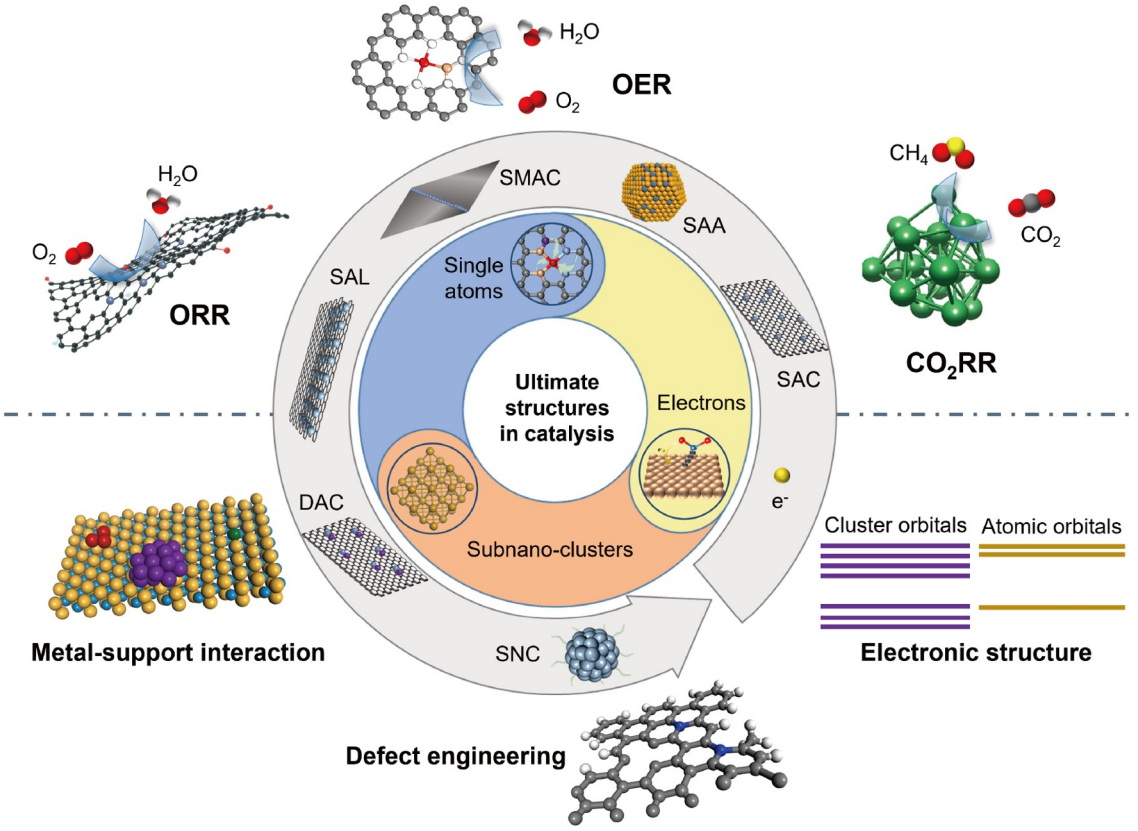

Figure 1 Ultimate structures in catalysis and modulating strategies.

ultimate structures of SACs, SMACs, and SALs characterized by SAs are depicted in Fig. 2.

Driven by the pursuit of increasing the number of active sites, SACs have received considerable attention. The strategies to enhance the properties of SACs, particularly the regulation of support species and defect engineering and the optimization of the coordination environment, serve as valuable guides for other kinds of catalysts with ultimate structures [16–18]. Studies of SMACs and SALs further highlight their exceptional advantages in increasing metal loading and harnessing synergistic effects between metal atoms compared with SACs [9,15]. In the subsequent sections, the distinctive features and recent efforts on SACs, SMACs, and SALs are summarized.

SACs

Since being proposed in 2011, SACs involving individually dispersed atoms on substrates have garnered remarkable attention [6]. By contrast to traditional catalysts in which only a fraction of metal atoms contribute to catalytic activity, the atomic dispersion of SACs is theoretically up to 100%, endowing SACs with maximized atomic usage efficiency and specific surface area [19–21]. Moreover, the distinctive electronic structure and controllable coordination environment are beneficial for enhancing the catalytic performance of SACs [22–25]. Notably, Pt SAs anchored on nitrogen-doped carbon nanosheets (Pt_1/NCNS) showed remarkable HER activity [26]. Compared with the counterparts with Pt SAs and nanoparticles, Pt_1/NCNS exhibits a similar HER activity while using significantly less Pt content. This notable performance of Pt_1/NCNS is attributed to its unique electronic structure, which features a higher unoccupied density of 5d orbital states than that of Pt nanoparticles. Zeolite-templated carbon with a substantial number of individually isolated Pt atoms undergoes a unique two-electron ORR pathway to produce H_2O_2, which could maintain high activity for 2 h [27]. Furthermore, Pt SAs on nitrogen-doped carbon (NC) effectively reduces the activation barrier of CO_2RR to 1.16 eV, facilitating the reduction of CO_2 to CH_4 [28].

Although extensive investigations of SACs have indicated their remarkable catalytic activity and scalability for large-scale preparation, further enhancements in metal loading and stability are required [29,30]. Constrained by the limited surface area of the supports and the high free energy of SAs, achieving metal loading exceeding 1 wt% is challenging for SACs [24,31–33]. As a result, although the catalytic activity of SAs can surpass that of nanoparticles by several folds, nanoparticles often exhibit a higher space-time yield than SACs [34,35]. Moreover, the high free energy contributes to the tendency of SAs to aggregate during the reaction and preparation processes [36]. Therefore, to enhance the catalytic performance, the metal loading and stability of SACs require to be increased compared with conventional catalysts. In particular, this enhancement can be achieved by the manipulation of support species and defect engineering and the optimization of the coordination environment.

Support species

Although SAs constitute the active sites in SACs, supports play an indispensable role during the reaction process [18,37]. Suitable supports help anchor and stabilize SAs while optimizing their catalytic performance through the MSI [38–40]. First, the surface properties of supports could control the catalytic beha-

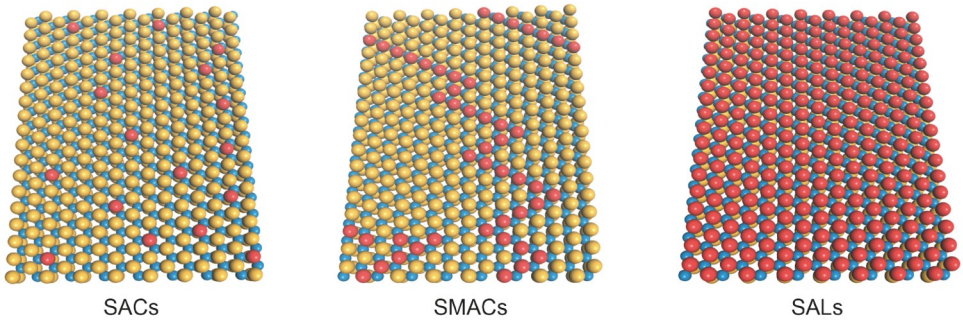

Figure 2 Schematic of SACs, SMACs, and SALs.

vior of SACs. Elements with strong electronegativity on the support surface, such as O, N, and S, are conducive to stabilizing SAs [41,42]. Unsaturated coordination environments of atoms on the support surface also provide strong interaction with SAs [43]. The oxidation–reduction property of the support surface is also related to the catalytic performance of SACs [44,45]. A study of Pt SAs on highly reducible Fe_2O_3, reducible ZnO, and irreducible γ-Al_2O_3 verifies that their catalytic performance is determined by the surface properties [45]. Pt SACs on supports with higher reducibility show a large turnover frequency (TOF) value for CO oxidation in the temperature range of 140–180°C. The modification of the surface properties of supports, such as doping, oxidation, and physisorption, has also been used in SACs [44,46,47]. Second, the functionalization of the support surface significantly influences the catalytic performance [48]. Functionalized support surfaces with attached groups have been observed to improve catalytic activity, stability, and selectivity. –OH functional groups on the aforementioned Fe_2O_3, ZnO, and γ-Al_2O_3 surfaces are significantly reduced during CO oxidation, increasing the CO oxidation rate of Pt SAs, particularly on the Fe_2O_3 surface [45]. Therefore, the influence exerted by the supports on SACs, particularly by the support species, requires to be thoroughly assessed.

Carbon-based supports impart diverse morphologies, porosity, and robust interfacial interactions to anchor SAs, rendering them the main representative category of SACs [49]. The large specific surface area inherent in porous carbon enables effective interactions with precursors, facilitating the capture of abundant SAs by doped atoms or geometric imperfections. Previous research shows that Fe SAs coordinated with N atoms in porous graphitized carbon (Fe-SA-NSFC) can attain a high metal loading of up to ~16 wt% (Fig. 3a) [50]. Conversely, the majority of the reported SACs exhibit metal loadings below 1 wt% [12]. The substantial loading of SAs on the porous support results in the exceptional ORR performance of Fe-SA-NSFC, outperforming commercial Pt/C catalysts. This approach also provides a general methodology to fabricate high-loading SACs with various SAs. Moreover, porous carbon supports offer various coordination structures, indicating their potential to enhance catalytic properties [51–53]. Pt precursors could be efficiently adsorbed by C and N atoms in nitrogen-doped porous carbon nanofibers (Pt-SA/pCNFs) [54]. The Pt-C_2N_2 coordination structure of Pt-SA/pCNFs exhibits a small negative binding energy, and Gibbs adsorbed free energy close to zero, indicating impressive HER activity and stability. Apart from ORR and HER, porous-carbon-based SACs have also been applied in other reactions, such as CO_2RR and N_2RR [55–57]. Porous carbon nanospheres are exploited to anchor single Fe atoms by electrostatic interaction [55]. The metal loading of the as-prepared Fe SACs is as high as 3.9 wt%, resulting in remarkable Faradic efficiency of up to 90%. Porous carbons also act as suitable substrates for stabilizing Mo SAs of Mo SACs [57]. Porous features and the large number of active sites endow this SAC with a superior NH_3 yield rate and enhanced durability. In studies of SACs for photocatalysis and thermocatalysis, the use of porous carbon is also indispensable. Ir SAs isolated by porous carbon nitride benefit from the synergism of interfacial carrier transfer [58]. Bonding between these Ir SAs and the support surface enable accelerated electron transfer and, in turn, decrease photocarrier transfer barrier. As a result, a remarkable conversion yield of CO_2 to methanol is achieved, even with a relatively low loading of Ir SAs (0.4 wt%). Mesoporous carbon foam nanospheres are used to anchor Pd SAs with large specific surface areas, resulting in higher thermocatalytic ethylene selectivity than Pd nanoparticles [59].

As a two-dimensional (2D) carbon material with distinctive geometry and electronic characteristics, graphene has been proven to be highly suitable for the deposition of SACs [63]. Similar to porous-carbon-based SACs, graphene-based SACs exhibit remarkable surface area. Moreover, the unique MSI and electronic characteristics lead to the distinctive advantages of graphene-based SACs [64,65]. The conjugated structure of graphene contributes to its elevated conductivity, thereby facilitating the rapid transport of electrons during chemical reactions [66–68]. Consequently, graphene-based SACs exhibit particular applicability in electrocatalysis, where the prompt transport of electrons is essential [69]. The location of coordination between graphene and adatoms also varies according to their species, ensuring precisely controllable catalytic performance of graphene-based SACs [64,70]. An example of graphene-based SAC with Co active centers (i.e., Co-N-C SAC) exhibits remarkable HER activity, as shown in Fig. 3b [60]. Co-N-C SAC exhibits enhanced intrinsic activity attributed to the preferential presence of low-coordinated Co-N_3 sites in the in-plane holes of graphene. This configuration results in a remarkably low Tafel slope (59 mV dec^{-1}) and overpotential (82 mV at 10 mA cm^{-2}), representing the smallest values reported to date. Because of the special bonding and electronic structure of isolated single Cu atoms on defective nanodiamond–graphene, effective activation of acetylene and easy desorption of ethylene are observed [71]. Thus, these graphene-based Cu SACs exhibit exceptional thermocatalytic selectivity (~98%) and activity for acetylene hydrogenation.

In addition to carbon-based SACs, research endeavors have

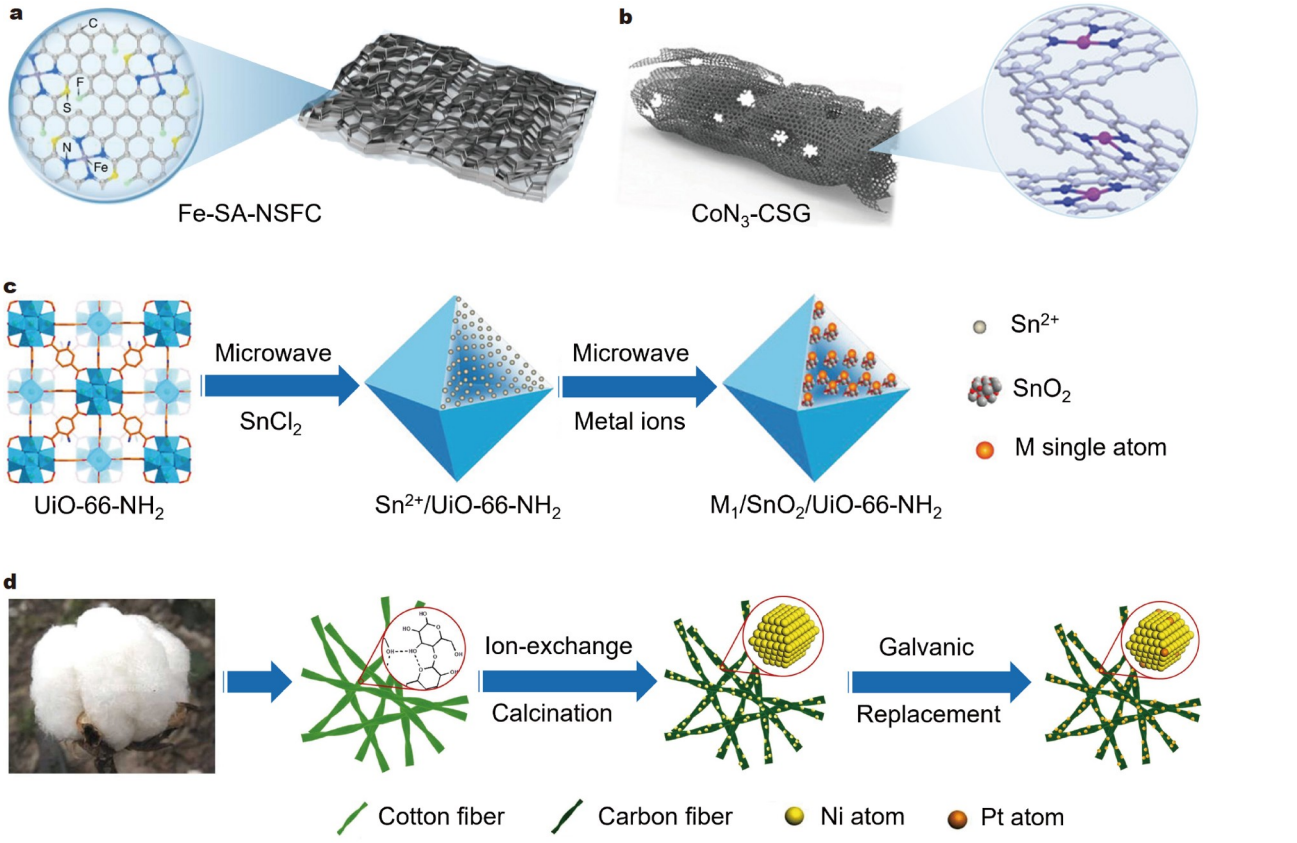

Figure 3 (a) Schematic of Fe-SA-NSFC. Reprinted with permission from Ref. [50]. Copyright 2020, Springer Nature. (b) Schematic of CoN_3-CSG. Reprinted with permission from Ref. [60]. Copyright 2022, Wiley-VCH. (c) Schematic of the microwave-assisted synthesis process for $M_1/SnO_2/UiO-66-NH_2$. Reprinted with permission from Ref. [61]. Copyright 2021, Wiley-VCH. (d) Schematic of the synthesis process for the fibrous PtNi/C catalyst derived from cotton. Reprinted with permission from Ref. [62]. Copyright 2022, Elsevier.

been significantly focused on the usage of metal-organic frameworks (MOFs) as support materials. As an emerging porous material with organic ligands and metal centers, MOFs exhibit a notable combination of characteristics, including large specific surface area, unsaturated metal sites, and abundant functional groups [72,73]. A general strategy is applied to deposit various SAs on SnO_2 trapped by MOFs (denoted as $M_1/SnO_2/MOF$, M = Pt, Cu, and Ni) *via* microwave-assisted impregnation and hydrolysis (Fig. 3c) [61]. Here, MOFs serve as ideal support with pore space and tailored microenvironment to increase SA loading, which decreases the proton activation barrier during the reaction. Consequently, the obtained $Pt_1/SnO_2/MOF$ exhibits noteworthy photocatalytic hydrogen production compared with that reported in previous studies. Moreover, the well-organized pore structure of MOFs contributes to heightened efficiency in electron transfer within SACs, thereby preventing the recombination of electrons and holes during reactions [74]. Zuo *et al.* [75] assembled Pt SAs coordinated with porphyrin precursors into MOF nanosheets by preparing 2D MOF-based SACs (PtSA-MNSs) for the first time. The as-prepared PtSA-MNSs exhibit the highest electron transfer efficiency relative to their counterparts, which contributes to their excellent hydrogen revolution rate reaching up to 11,320 $\mu mol\ g^{-1}\ h^{-1}$. Furthermore, MOFs exhibit a high degree of controllability in terms of diverse aspects, including pore size, coordination sites, and the constituents of precursors [76,77]. For instance, 3D hybrid MOFs enable Co SAs to find a suitable coordination environment for reducing the free energy of ORR, thereby enhancing the catalytic activity [78]. The SACs based on MOFs have also exhibited exceptional performance in photocatalysis, such as photocatalytic CO_2RR. Gas-permeable MOF membranes are effective substrates to facilitate gas diffusion, thereby improving the performance of Ir SAs in photocatalytic CO_2RR [79–81].

Recently, biomass materials have gained prominence as sustainable and cost-effective supports for SACs [82–84]. A substantial portion of biomass precursors exhibit hierarchical and porous structures to anchor abundant SAs, obviating the need for energy-consuming synthesis processes [85,86]. A green method uses cotton as an *in situ* support for facilitating the anchoring of atomically dispersed Pt (Fig. 3d) [62]. The catalytic activity of the obtained SAC was determined to surpass that of the primary Ni/C catalyst by approximately 25 times. The cost efficiency of cotton enables the industrial application of Pt SAC. Moreover, the use of abundant biomass substrates from the earth leads to eco-friendly methodologies for large-scale SAC preparation [87,88]. Zhong *et al.* [89] synthesized Fe-N-C catalysts on wood-based porous carbon by using a scalable method for SAC preparation. The hierarchical structure of the cell wall in wood after pretreatment increases their ORR/OER activity and durability.

Apart from carbon-based SACs, metal-based SACs also have promising potential in various catalytic reactions. Single-atom alloys (SAAs) with atomically dispersed SAs on the surface of metallic supports have unique properties [90]. This structure not

only presents the merits of SACs but also inherits the synergistic effect characteristics of alloys [17,91]. Different from that in traditional alloys, previous studies reported that the electronic structure of the dopant element in SAAs is similar to that of free atoms. The density of state (DOS) was measured to explore the electronic structure of the dopant element Cu in AgCu SAA [92]. The results indicate that the d-band of Cu exhibits atomic-level narrowness, similar to that of a free atom. Analogous d-orbital projected DOS profiles were observed in diverse dopant elements on Au host metal, verifying the presence of free-atom-like electronic states in SAAs [93,94]. This distinctive electronic structure endows SAAs with the capability to modulate the reaction mechanisms, particularly the adsorbate bonding [94,95]. The diminished density of d-electrons in Pt SAAs weakens the Pt–CO interaction, subsequently reducing the adsorption energy of CO on the surface [93]. Consequently, this reduction in adsorption energy hinders the self-poisoning of Pt SAAs. The high atomic usage and catalytic activity of SAs in SAAs can also contribute to the reduction in noble metal expenditures during catalyst preparation, resulting in an effective approach for the efficient utilization of noble metals. A Cu-based Au SAA with surface Cu vacancies (V_{Cu}-Au_1Cu SAAs) was synthesized by galvanic replacement [96]. In V_{Cu}-Au_1Cu SAAs, the generation of electron-deficient Cu sites is facilitated through the migration of electrons from Cu to Au. Despite the limited quantity of Au SAs on the Cu surface, V_{Cu}-Au_1Cu SAAs exhibits desirable activity for the electroreduction of NO_3^- to NH_3. Recently, SAA with Ru SAs on a Co substrate (Ru_1Co-SAA) has been found to photohydrogenate CO into liquid fuels with outstanding conversion and selectivity, surpassing the performance of Co nanoparticles [97].

The SACs on metal oxides have also been widely investigated [98,99]. TiO_2, a metal oxide semiconductor, is a representative example of this field. For Ir SAs on defective TiO_2 (Ir_1/def-TiO_2), the interaction between SAs and metal supports was verified to optimize their electronic and geometric structures [100]. As a result, Ir_1/def-TiO_2 shows remarkable performance in the thermocatalytic hydrogenation of furfural to furfuryl alcohol, surpassing that of Ir SAs on graphitic carbon nitride substrates. The photocatalytic HER performance of SAs on different TiO_2 surfaces indicates that the (001) surface exhibits enhancement in capturing SAs by strengthening the MSI, which results in improved proton adsorption and reduction [101]. Researchers found that improving the catalytic performance of SACs by anchoring SAs to favorable metal facets is a practical approach, which is difficult to conduct in carbon supports. Furthermore, CeO_2 supports have been analyzed in depth to explore the influence of structural and electronic dynamics on SACs, which are essential for increasing catalytic activity and stability [102,103].

In summary, appropriate supports render stable SAs with high metal loading and strong MSI, which are conducive to optimizing catalytic performance. As the largest category of SACs, carbon-based SACs have enabled numerous developments in catalysis, in which porous carbon, graphene, MOF, and biomass materials play impressive roles. Moreover, SAAs with metal supports have unique catalytic properties, particularly the synergistic effect.

Defective structures

As extensively existing structures in catalysts, defects have a significant influence on the preparation process and reaction mechanism of SACs. During the preparation process of SACs, various defects emerge as essential factors in stabilizing high-loading SAs by anchoring active sites and strengthening the MSI [46,104]. Vacancies, dopants, and edge defects represent prevalent defect types commonly harnessed in SAC preparation. Vacancies could capture SAs through their affinity with their neighboring atoms. Liu *et al.* [105] introduced carbon vacancies to NC nanosheets by thermal etching and, in turn, confined Pd SAs using these carbon vacancies. The formation of Pd-N_3 sites is pivotal for ensuring the stability of individual Pd atoms. Similarly, vacancies in graphene have been harnessed to trap diverse SAs [47,106]. Through pyrolysis, carbon vacancies are intentionally induced in graphene, showing remarkable capability to capture isolated Pt atoms (Fig. 4a) [106]. Pt SAs trapped by carbon vacancies further form Pt-C_3 active sites, exhibiting robust electron capture capability and reduced Gibbs free energy difference. Consequently, Pt-C_3 sites show exceptional HER activity, with a TOF value of 1584.6 h^{-1} and a mass activity of 26.05 A g^{-1}.

Doping provides an alternative approach for preparing SACs by defect engineering [109]. Extensive researches on nonmetallic dopants with lone-pair electrons, such as N, O, and S atoms, have yielded insights into their capacity to capture individual metal atoms through chemical bonding. A notable example of doping is preparing a durable Ni-N-C SAC to address the inherent vulnerability of Ni catalysts under acidic conditions [110]. The chemical bonding between Ni and neighboring N atoms leads to its exceptional stability, even in the presence of hot water and tungstic acid. Furthermore, the strong electronegativity of O atoms enables them to anchor single Ni atoms onto graphene, thereby forming Ni-O_6 coordination sites (Fig. 4b) [41]. Because of the remarkable activity of Ni SAs and the weak Ni–O bonds, this Ni SAC exhibits excellent HER performance in an alkaline environment. Moreover, the metal loading of Ni SAs correlates with the number of O defects, providing a facile strategy to modulate their OER performance by controlling the applied voltage or electrolytes. Doping can also induce other types of defects, such as vacancies, to construct SAs. The introduction of abundant Mg^{2+} vacancies through Al^{3+} doping plays a significant role in isolating single Cu atoms, achieving loadings of Cu atoms of up to 6.3 wt% [111]. By contrast, without Al^{3+} dopants, Cu atoms tend to aggregate into nanoparticles.

Another commonly existing defect type, i.e., edge defects, has promising potential for SAC preparation. Serving as an intrinsic defect component, edge defects provide distinctive structural and electronic environments conducive to anchoring SAs [112,113]. Experimental findings have confirmed the capability of the monoatomic step edges in CeO_2 to capture, stabilize, and manipulate Pt^{2+} SAs [114]. The manipulation of step density maximizes the Pt^{2+} coverage of step–edge sites to 80%. Analogous outcomes were obtained in studies of carbon-based SACs [115,116]. Exploiting the edge defects of mesopores in graphene enables the capture of Mo SAs, which is crucial for fabricating oxygen- and sulfur-doped graphene (OSG) hosting Mo SAs (Mo_1/OSG) [116]. Because of the capability of the defective edges to stabilize SAs, the metal loading of Mo_1/OSG is as high as 10 wt%.

Defects exert a profound influence not only on SAC preparation but also on the underlying chemical reaction

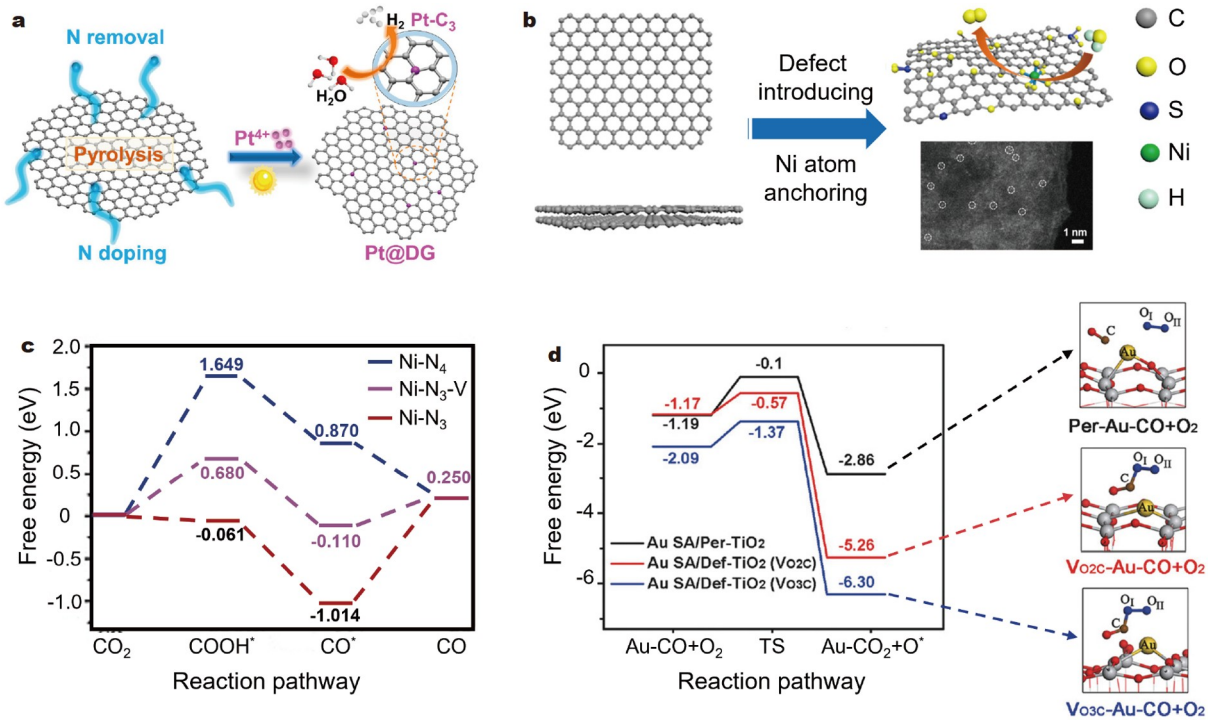

Figure 4 (a) Schematic of Pt SAs captured on carbon vacancies by pyrolysis. Reprinted with permission from Ref. [106]. Copyright 2022, American Chemical Society. (b) Schematic of the process of inducing defects and anchoring Ni atoms to generate Ni SAC. Reprinted with permission from Ref. [41]. Copyright 2020, American Chemical Society. (c) Calculated free energy diagram illustrating the conversion of CO_2 into CO on Ni-N_4, Ni-N_3-V, and Ni-N_3. Reprinted with permission from Ref. [107]. Copyright 2020, Wiley-VCH. (d) Schematic models depicting the CO oxidation process of Au SAs on perfect, O_2C, and O_3C defective TiO_2 (001) surfaces. Reprinted with permission from Ref. [108]. Copyright 2018, Wiley-VCH.

mechanisms. The active sites formed by defects could influence the energy path during catalytic reactions because of their structural alterations [117,118]. Rong *et al.* [107] conducted a seminal study of Ni SACs with vacancy defects (Ni-N_3-V SAC) and perfect supports (including Ni-N_3 and Ni-N_4 SACs) with diverse configurations by performing density functional theory (DFT) calculations on these structures. The DFT result of CO_2 reduction to $COOH^*$, the rate-determining step of CO_2 reduction, indicates that vacancy defects substantially diminishes the energy barriers for $COOH^*$ and desorbing CO compared with Ni-N_4 sites (Fig. 4c). Although Ni-N_3 sites show favorable Gibbs energy difference at the initial steps, the pronounced discrepancy of their Gibbs energy at the fourth step impedes efficient CO_2RR. Consequently, the Ni-N_3-V SAC exhibits superior catalytic performance in CO_2RR than in Ni SAC without defects. The DFT calculations of Ni SACs on NC supports (Ni-SAC@NCs) present similar results [119]. Ni-SAC@NCs exhibits an extraordinarily low free energy barrier (0.62 eV) for $COOH^*$ generation from CO^*, which is the pivotal step for CO_2RR. This remarkable CO_2RR efficiency is attributed to the favorable defect-enriched configuration. Moreover, defective structures induce changes in adsorption processes arising from steric hindrance effects, electrostatic influences, and perturbations in electronic structures [120]. Notably, single Au atoms anchored on TiO_2 nanosheets with oxygen vacancies (Au-SA/Def-TiO_2) exhibit distinct behavior [108]. In this SAC, Au SAs are stabilized by the three-center Ti-Au-O-Ti structure. Because of the large interfacial steric hindrance effect and the electrostatic repulsion caused by the surface oxygen atoms, CO adsorption on Ti atoms is weaker than that of Au SAs on perfect TiO_2 nanosheets (Au-SA/Per-TiO_2) (Fig. 4d). By contrast, Au-SA/Def-TiO_2 with oxygen vacancies exhibits heightened CO adsorption at Ti sites, alleviating the competitive adsorption between O_2 and CO. Furthermore, the energy barrier of Au-SA/Def-TiO_2 is reduced. This dual advantage attributed to oxygen vacancies collectively improves the catalytic CO oxidation process in Au-SA/Def-TiO_2. Thus, the influences of defects on the preparation process and reaction mechanism significantly enhance the catalytic performance of SACs, including stability, selectivity, and activity [121,122].

In summary, defects have been considered an indispensable factor in capturing, stabilizing, and manipulating SAs. The precisely tuned microenvironment of SACs by defective structures has promising potential in tailoring catalysts. To realize the large-scale preparation of defective SACs, energy-efficient methods to create defects are crucial and need to be further investigated.

Coordination environments

The coordination environment has a profound influence on the electronic structure of SAs, serving as an indispensable factor affecting the stability, selectivity, and activity of SACs [123–125]. The coordination environment is divided into geometric and chemical aspects, with the latter including local composition and coordination numbers (CN). The local composition influences the catalytic performance of SACs by tuning the adsorption configuration during reactions. Ru SACs captured on different cation vacancies of NiFe-layered double hydroxides (Ru_1/LDH-V_{II} or Ru_1/LDH-V_{III}) were synthesized to reveal the influences of diverse coordination environments (Fig. 5a) [126]. The obtained

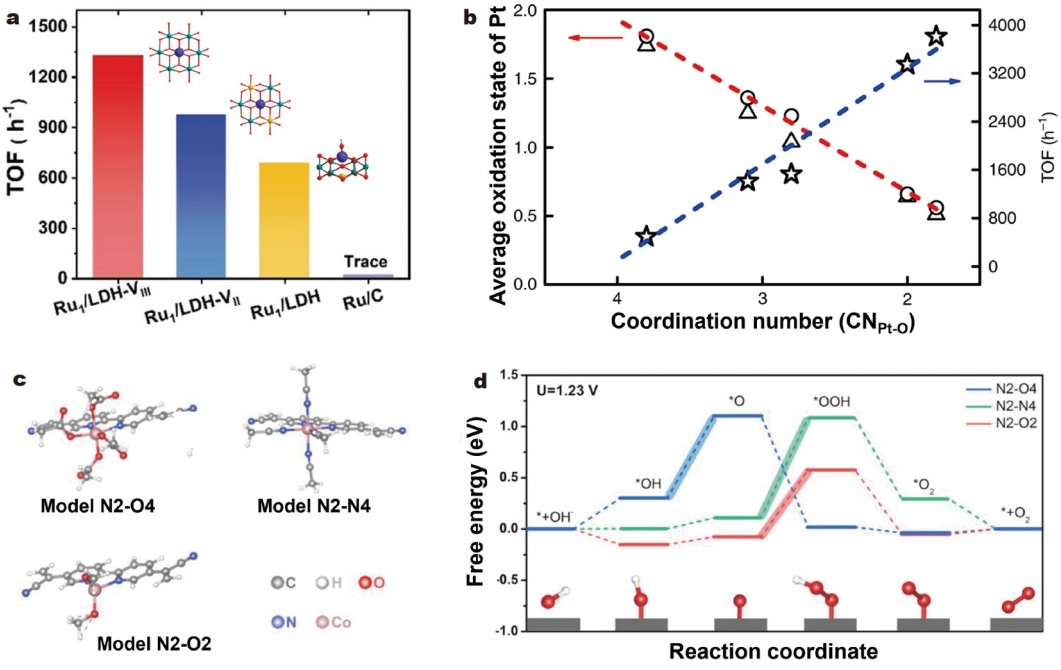

Figure 5 (a) Schematic of $Ru_1/LDH\text{-}V_{II}$, $Ru_1/LDH\text{-}V_{III}$, and Ru_1/LDH with different coordination environments and corresponding TOF values. Reprinted with permission from Ref. [129]. Copyright 2021, Wiley-VCH. (b) Linear correlations between the CN of Pt–O and the average oxidation state (red line) and between the CN of Pt–O and the hydrogenation activity (blue line) of Pt_1/Fe_2O_3. Reprinted with permission from Ref. [128]. Copyright 2019, Nature Publishing Group. (c) Potential models for three out-of-plane configurations of Co SACs. (d) Schematic of free energy over three models at 1.23 V for OER. Reprinted with permission from Ref. [130]. Copyright 2022, Wiley-VCH.

Ru SAs on cation vacancies and surface sites were generally classified as +4 and 0–+3 states, respectively. Differential coordination environments were also observed for Ru SAs anchored by LDH-M_{II} or LDH-M_{II}. Notably, Ru atoms anchored by LDH-M_{III} exhibit a higher oxidation state and fewer d-state electrons than Ru atoms anchored by LDH-M_{II}, leading to benzaldehyde desorption. As a result, differences in the coordination environments lead to diverse catalytic performance, with the Ru SAs captured by LDH-M_{II} vacancies exhibiting the highest efficiency of benzyl alcohol oxidation (TOF value of 1331 h^{-1}) among these samples.

The influence of CN on catalytic performance was exemplified in single Pt atoms on N-doped carbon with different CNs (Pt_1-N_xC_y) [127]. Four-coordinated single Pt atoms exhibit lower formation energy than three-coordinated single Pt atoms, indicating a preference for dispersion over aggregation. Compared with Pt_1-N_1C_2 with 3CN, 4CN Pt_1-N_1C_3 has a weaker Pt–N hybridization, corresponding to a higher Pt-5d center. The elevated 5d center optimizes the hydrogen dissociation energies, enabling 4CN Pt_1-N_1C_3 to increase hydrogenation activity. When the CN of Pt–O decreases, the oxidation state for Pt SAs on Fe_2O_3 (Pt_1/Fe_2O_3) exhibits a proportional decrease (Fig. 5b) [128]. This shift in the Pt oxidation state further boosts the hydrogenation activity of Pt_1/Fe_2O_3 (TOF value of up to 21,099 h^{-1}) while preserving its selectivity (95%–98%). These studies reveal the potential for enhancing catalytic performance by manipulating the CN of SAs.

Tuning the geometric structure of the coordination environment has emerged as a viable strategy to improve the catalytic performance of SACs. For instance, the OER performance of three out-of-plane configurations (with potential models of N2-O4, N2-N4, and N2-O2) was investigated on Co SACs, extending the scope of geometric exploration to the coordination environment (Fig. 5c) [130]. The evaluation of these configurations reveals variations in the energy barriers for *OOH formation from *O, the rate-determining step (Fig. 5d). Consequently, diverse OER performance is achieved in different configurations. Specifically, the N2-O2 model shows the lowest energy barrier for the rate-determining step, resulting in exceptional mass activities and TOF values for this specific configuration.

In summary, the nature of support species, the presence of defect structures, and the coordination environments collectively exert pivotal influences on the catalytic properties of SACs. The feasibility of designing SACs by modulating these factors is worth investigating. Furthermore, the influences of these parameters highlight the significance of the ultimate structures in catalysis. The ultimate structure of SACs exhibits not only the indispensable role of SAs but also the profound differences in catalytic performance yielded by even slight alterations at the atomic scale.

SMACs

To improve the metal loading and modulate the electronic structure of catalysts with ultimate structures at an advanced level, the exploration of incorporating several atoms in an active center while preserving a low-dimensional structure represents a promising avenue [131]. 1D catalysts have emerged as a favored platform for catalytic applications because of their distinctive high aspect ratio and confined carrier transport pathways [132,133]. A notable example of such materials is the Fe–N-doped carbon nanofibers (Fe-NHCFs) synthesized as a typical kind of 1D carbon catalysts for ORR [134]. The pronounced specific area arising from the inherent 1D configuration equips

Fe-NHCFs with numerous active sites; meanwhile, electron transfer is facilitated using the 1D honeycomb-like conductive networks. As a result, Fe-NHCFs exhibit a current density of 5.2 mA cm^{-2} at 0.70 V (*vs.* reversible hydrogen electrode (RHE)), a notable advancement compared with 5 mA cm^{-2} for the conventional 20 wt% commercial Pt/C catalyst. Similar circumstances were observed in Fe–N-doped 1D porous carbon nanotubes [135]. These nanotubes exhibit an impressive surface area of 1380 cm^2 g^{-1} and electron transport expedited by the 1D structure. Subsequently, these nanotubes show remarkable ORR activity throughout a long-time test, surpassing the performance of the commercial Pt/C catalyst. However, the conventional 1D catalysts have not comprehensively emphasized or modulated the critical role of SAs, thereby rendering the regulation of catalytic performance from an ultimate structure perspective a challenge.

As a special kind of catalyst with ultimate 1D structure in the scale of SAs, SMACs not only inherit the advantages of 1D catalysts but also can harness the unique benefits of SAs. Being the smallest 1D structures formed by atoms arranged along a single direction, SMACs offer a promising avenue for generating a large number of active sites by increasing the specific surface area. Previous research has reported that the average bond strength of SMACs is twice that of bulk materials, indicating the stability of SMACs in chemical reactions [136]. The 1D structure of SMACs facilitates rapid electron transport through the oriented pathway, thereby enhancing their catalytic activity [137,138]. Furthermore, the electron transport properties of SMACs are different from those of other catalysts with ultimate structures because of the phenomenon of quantized conductance, indicating the potential for novel catalytic mechanisms to emerge [139,140].

The introduction of Ag atoms to the tunnels of Hollandite-type manganese oxide (HMO) to form Ag SMACs exemplifies the use of the concept of SMACs [7]. Transmission electron microscopy (TEM) and high-resolution TEM (HRTEM) images confirm the structure of Ag-HMO nanorods and Ag SMACs, respectively (Fig. 6a, b). Theoretical models depict Ag chains and terminal Ag SAs from two distinct perspectives (Fig. 6c, d). The terminal Ag SAs exposed at the top facets of HMO become active sites for HCHO oxidation, exhibiting superior capability to activate oxygen species even at low temperatures. Although studies of SMACs in catalysis are relatively limited to date, their catalytic potential remains appealing because of the advancements in their synthesis methods [15,141]. Pt SMACs with a high density, i.e., exceeding 10 wt%, were synthesized by the vapor co-deposition method [15]. Fig. 6e shows the annular dark-field scanning TEM (ADF-STEM) image of one obtained Pt SMAC. The magnified ADF-STEM image of a rectangular region in this Pt SMAC indicates that an atomically coherent 1D channel is formed (Fig. 6f). These observations reveal the well-ordered nature of Pt SMACs, as detailed in the model shown in Fig. 6g. During the deposition process, the grain boundaries of MoS_2 provid anchor sites for stabilizing Pt SMACs, resulting in an average length of up to 17 nm for high-density Pt SMACs. This synthesis strategy provides a general approach to fabricating high-density SMACs, with the potential to incorporate a multitude of active centers in catalysts with ultimate structures. Furthermore, Pt SMACs exhibit exceptional stability in ambient air, which is beneficial for prolonging the lifetime of catalysts.

Although previous studies have highlighted the promising potential of SMACs in catalysis, several challenges persist, par-

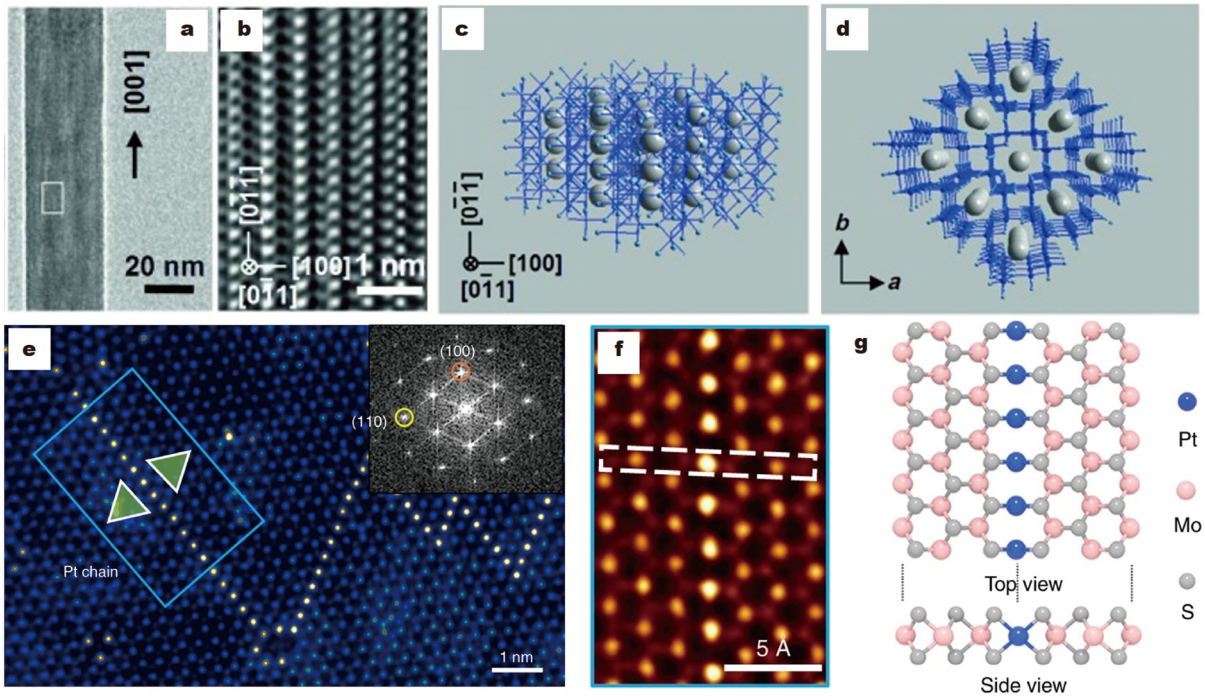

Figure 6 (a) TEM image of Ag-HMO nanorod along the growth direction of [001]. (b) HRTEM image revealing the Ag SMACs. (c) Schematic of Ag SMACs inside the tunnels of HMO in the direction of [0$\bar{1}$1]. (d) Schematic of Ag SMACs inside the tunnels of HMO viewed from [001], indicating the terminal SAs. Reprinted with permission from Ref. [7]. Copyright 2022, Wiley-VCH. (e) False-colored ADF-STEM image of a Pt SMAC. Inset: a fast Fourier transformation of the blue rectangular area. (f) Magnified ADF-STEM image of a Pt SMAC. (g) Schematic of the detailed atomic structure of Pt SMAC. Reprinted with permission from Ref. [15]. Copyright 2022, Springer Nature.

ticularly in achieving controllable preparation methods for SMACs and enhancing their density. Notably, the exposed atoms in SMACs, which could facilitate the engagement of a larger number of active sites in catalytic reactions, need to be increased, thereby further optimizing their performance.

SALs

With the tendency to increase the metal loading for ultimate structures in the scale of SAs, current research endeavors are directed toward developing SALs, which is the smallest 2D ultimate structure [142–144]. SALs are composed of metal atoms arranged in monolayer, with thicknesses limited to approximately 1 nm [9]. The fundamental characteristic of SALs is the complete exposure and activation of atoms, leading to an ultrahigh density of active sites. This feature ensures that SALs achieve satisfactory catalytic performance. He *et al.* [8] used ion etching under low-density plasma at −30°C to remove Se atoms from predeposited 2D $PtSe_2$, synthesizing Pt SAL with an amorphous structure (Fig. 7a). After the synthesis process, an assessment of the catalytic efficacy of the obtained Pt SAL was conducted. With the increase in Se vacancies during etching, an enhancement in the current density of HER in Pt SAL was observed (Fig. 7b). Initially, the basal plane of the perfect single crystal is HER inert. After plasma etching for a short time, defective $PtSe_x$ exhibits moderate HER performance, with an onset potential of ~0.1 V (*vs.* RHE) and a Tafel slope of ~100 mV dec^{-1}. Finally, a notable increase in the current density to 25 mA cm^{-2} at 50 mV (*vs.* RHE) in Pt SAL, accompanied by a reduction in the Tafel slope to 39 mV dec^{-1}, is achieved. The scope of SAL extends to studies of alloys. As an illustration, an atomically thick Pt–Cu nanosheet was fabricated in a sandwich structure configuration [145]. This nanosheet exhibits remarkable activity in formic acid oxidation.

An appealing approach to advancing the field of SALs is the preparation of freestanding SALs. Theoretically, atoms in freestanding SALs have dangling bonds in one dimension while maintaining coordination bonds in other dimensions [146]. Thus, freestanding SALs exhibit a higher energy band in one dimension because of the split of its empty valence band in this 2D coordination environment. This unique structure empowers freestanding SALs to achieve unusually remarkable activity in catalysis. Conversely, within the plane formed by the two other dimensions, atoms are stabilized through coordination bonds, indicating the inherent stability of freestanding SALs. For instance, although orbital splitting is challenging to discern in Pd SAL because of the weak Pd–Pd interaction, it becomes distinctly evident in the case of PdCo SAL because of the robust Pd–Co interaction (Fig. 7c) [146]. For PdCo nanoparticles and Pd few-atom layers, the electronic interference lacks directional preference, leading to the presence of conventional orbitals. As a result, in an accelerated durability assessment spanning the range of 0.6–1.1 V (*vs.* RHE), PdCo SAL only shows reductions in the electrochemically active surface areas by 8.8%, whereas the 3D Pd catalyst exhibits a substantial decline as high as 67.9%. Moreover, PdCo SAL exhibits a mass activity six times higher than that of commercial Pt NP catalysts. The exceptional activity

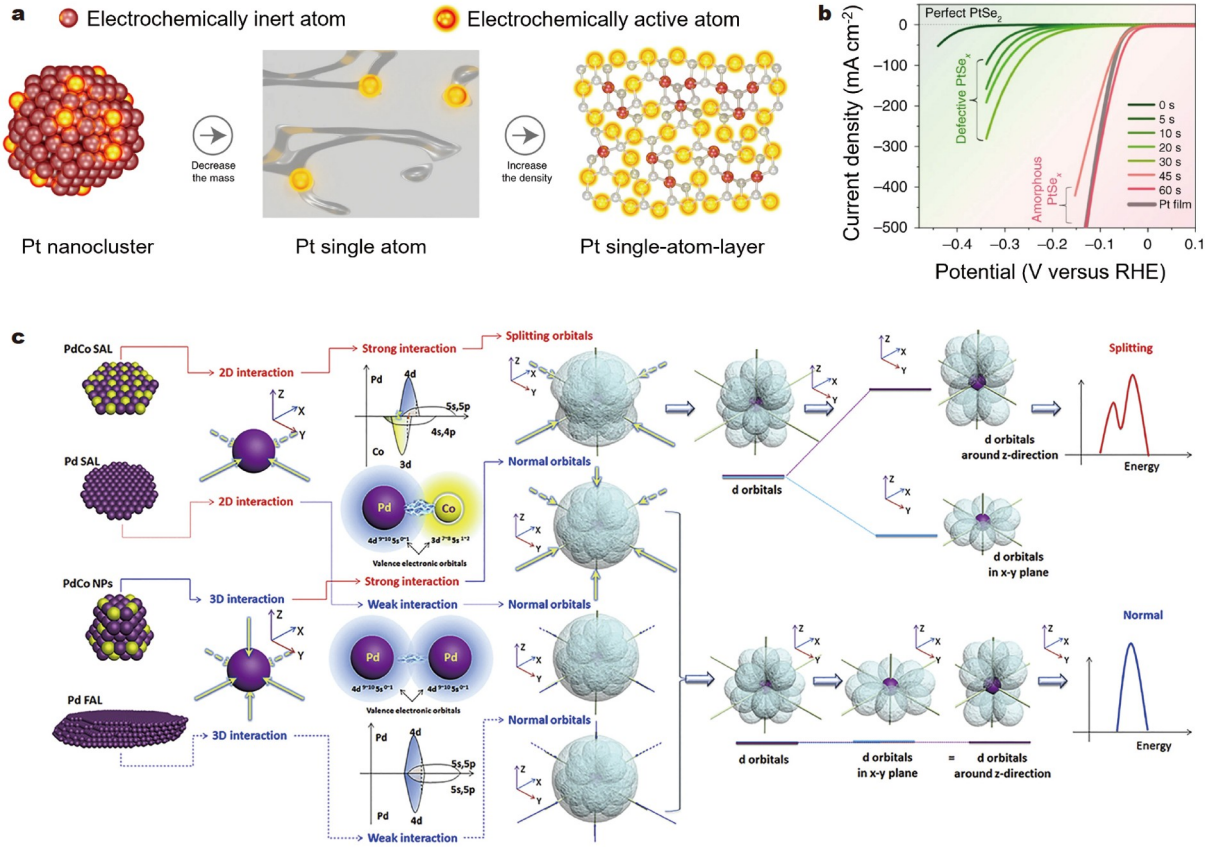

Figure 7 (a) Schematic of the structural evolution of Pt catalysts from SNCs to SAs and SALs. (b) Polarization curves of $PtSe_x$ as the treatment duration spans from 0 to 60 s, corresponding to varying x values from 2.0 to 1.1. Reprinted with permission from Ref. [8]. Copyright 2022, Springer Nature. (c) Schematic of the 2D-oriented coordination in the SAL. Reprinted with permission from Ref. [146]. Copyright 2019, Elsevier.

and durability of PdCo SAL indicate the significance of the distinctive electronic structure inherent to SAL.

Although SALs exhibit remarkable strength in catalysis, increasing the proportion of activated atoms is a challenge in preparing SALs. For most 2D catalysts, only atoms at the edge are activated, leaving other areas of the monolayer uninvolved in the reaction. Moreover, parameters that regulate active sites, including defects, substrate species, and coordination environments, play a pivotal role in advancing SALs [146–148]. Notably, the confinement effect of the oxygen vacancies was used to prevent Pt atoms from aggregating, which is beneficial for anchoring Pt SAL [147]. This Pt SAL exhibits an outstanding hydrogen evolution rate of 25.5 μmol cm^{-2} h^{-1} and stability for up to one week.

ULTIMATE STRUCTURE II: SNCs

Ultimate structures in the scale of SAs have remarkable advantages, such as maximized atomic utilization efficiency, large specific surface area, and unsaturated coordination environments. However, their progress in catalysis is inherently constrained by the structure of single active centers. For SACs, the restrictions in metal loading, linear relationship, and electronic structure are inevitable. Metal loading lower than 1 wt% has impeded catalytic application for a large proportion of SACs [24,31–33], as discussed in *SACs*. Overcoming this challenge within SACs remains a complex task because of the ultrahigh free energy of SAs. Moreover, all intermediates of SAC are bound in the same active site during the reaction. Previous studies have indicated that this situation will lead to a linear relationship between intermediate and adsorption energy [149]. However, a tradeoff arises between activation and desorption, which means that the linearly varying adsorption energy makes it difficult for SACs to modulate the reaction pathway [150]. Moreover, although the electronic structure of active sites in SACs could be modulated by supports and defects, the inherent simplicity of the SAC structure limits the efficacy of such modulation, particularly in sophisticated reactions [151]. For SMACs and SALs, the research is still in the initial stages. The development of refined synthesis and activation methodologies for SMACs and SALs requires further exploration [7,9].

To solve the aforementioned challenge of SACs, a range of strategies involving synergistic effects and dynamics have been pursued [152]. As a cross-dimensional extension of ultimate structures in the scale of SAs, SNCs have emerged as a promising avenue for addressing these issues. SNCs (smaller than their threshold sizes of quantum size effect, generally <2 nm in size) are composed of dual atoms to dozens of atoms (Fig. 8a), constituting a distinctive category of ultimate structures in catalysis

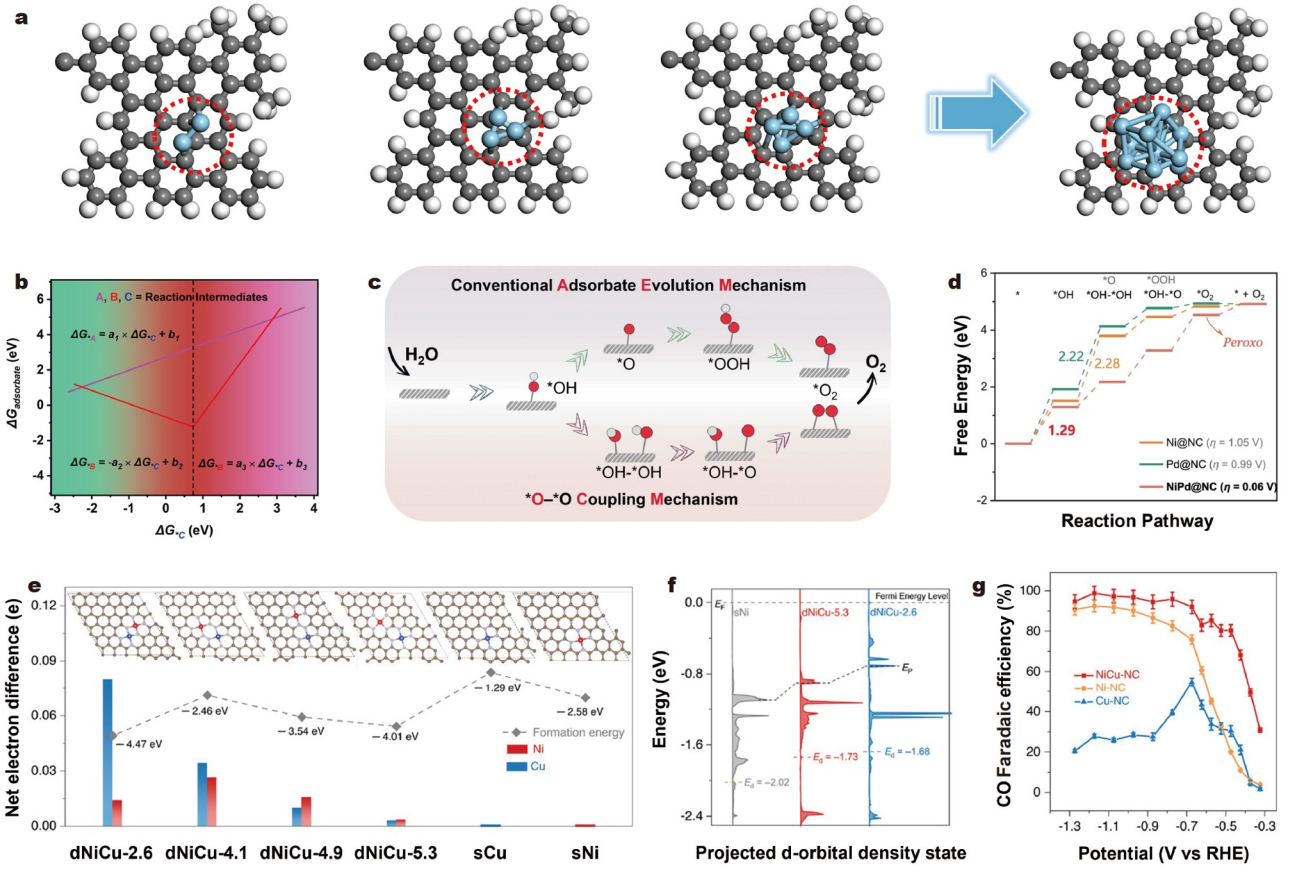

Figure 8 (a) Schematic of SNCs with different numbers of atoms. (b) Linear relationship of the free energy of adsorption of intermediates in SACs. Reprinted with permission from Ref. [157]. Copyright 2022, American Chemical Society. (c) Schematic of the conventional adsorption evolution and $^*O$–$^*O$ coupling mechanisms. (d) Gibbs free energy diagram of NiPd@NC and the corresponding SACs for OER. Reprinted with permission from Ref. [158]. Copyright 2023, Springer Nature. (e) Net electron difference of Ni and Cu sites in different dNiCu models using Ni SAC (sNi) and Cu SAC (sCu) models as the baseline, respectively. (f) Comparison of the free energy diagrams of Ni sites for the dNiCu-5.3, dNiCu-2.6, and sNi models under HER. (g) Potential-dependent Faradaic efficiencies of CO for NiCu-NC, Ni-NC, and Cu-NC. Reprinted with permission from Ref. [159]. Copyright 2023, Wiley-VCH.

[10]. The significant feature of SNCs is the quantization of the conduction band, which enables them to exhibit different electronic properties in comparison with nanoparticles (>2 nm) with a relatively continuous valence band [153]. Au SNCs have been investigated as a typical example of SNCs for decades, exhibiting considerable electronic relaxation when changing from Au nanoparticle (15 nm) to Au_{55} SNC (1.4 nm) [154]. The decrease in electronic relaxation continues as the size reduces to 0.7 nm in Au_{13} SNC, which further highlights the difference between SNCs and nanoparticles. Furthermore, significant advancements in terms of increasing metal loading, breaking linear relationships, and modulating electronic structure have been observed in SNCs [4,151,155]. Consequently, SNCs have exhibited exceptional catalytic performance compared with ultimate structures with SAs [10,156]. The origins and current developments of these strengths of SNCs will be subsequently discussed.

Why SNCs?

Compared with SACs, SNCs exhibit distinctive properties, such as increased metal loading, the disruption of linear scaling relationships, and enhanced electronic structures, as previously discussed [156,160]. In SNCs, each active site comprises multiple metal atoms, leading to higher metal loadings compared with SACs, even with an equivalent number of active sites. Furthermore, because of the interactions between adjacent atoms, the formation energy of multiatom sites generally tends to be lower than that of SACs, indicating that the multi-atom configurations in SNCs are inherently considerably stable [11,161]. Moreover, compared with SMACs and SALs that need to be precisely prepared, SNCs have advantages in simplifying the synthesis process [162,163]. These inherent features collectively contribute to the facilitated increase in metal loading for SNCs. For instance, Wei *et al.* [164] prepared Fe dual atoms on graphitized N-doped carbon layers. Theoretical calculations validate that the formation energy of dual Fe configurations is lower than that of Fe SAs, indicating a propensity for higher metal loading with Fe.

The optimized adsorption configuration and reaction pathway lead to the breakage of the linear relationship in SNCs. A representative linear relationship of the free energies of adsorption between intermediate C and other intermediates of SACs is shown in Fig. 8b, where the simple structure of active sites makes it difficult to modulate the free energy of adsorption [157]. By contrast, active centers in SNCs are composed of multiple adjacent atoms, enabling reactants to not only bond with diverse elements but also simultaneously engage with multiple atoms during reactions [165,166]. This structure allows SNCs to surpass the constraints of bonding with only the same atom in SACs for reactants, particularly during complex reactions. Therefore, SNCs can provide a broad range of adsorption configurations, thus enhancing their potential to improve catalytic performance. Fang *et al.* [158] investigated a series of dual-atom catalysts (DACs, referred to as M′M@NC) to unravel their reaction pathways. In the conventional adsorption evolution mechanism (AEM), the binding energies of intermediates exhibit strong correlations. However, the $^*O$–$^*O$ coupling mechanism (OCM) with a second active center breaks this structural constraint in AEM. In OCM, the pathway of O_2 production circumvents the $^*OOH$, thereby enabling M′M@NC to avoid the linear relationship (Fig. 8c). As a result, all M′M@NC samples exhibit superior OER activity compared with the corresponding SACs. A notable illustration is provided by NiPd@NC, where the Gibbs free energy barrier for OER is significantly reduced compared with those of Ni@NC and Pd@NC (Fig. 8d).

Because of the presence of additional metal atoms within the active centers, SNCs provide a broad range of avenues for enhancing catalytic performance compared with SACs, particularly the modulations to optimize electronic structures [167–169]. The interactions between multiple atoms within SNCs lead to a coupling effect on electronic structures, thereby modulating d-band structures and charge densities accordingly [170]. Moreover, the unique microenvironment of SNCs renders them sensitive and adaptable to tailoring electronic structures in response to different intermediates [171,172]. The distinctive electronic structures of SNCs could be revealed through investigations on NiCu dual atoms on NC (NiCu-NC) [159]. When the inter-metal distance falls below a critical threshold (5.3 Å), the decrease in the inter-metal distance leads to a strongly altered electronic structure for metal centers (Fig. 8e). Simultaneously, the DOS for NiCu-NC shows a marked upshift of the d-band center with the decrease in the inter-metal distance (Fig. 8f). This controlled electronic structure in the threshold-distributed NiCu-NC enhances the adsorption of CO_2 during electroreduction, resulting in a lower onset potential (300 mV) and a broader potential window (~800 mV) than the counterparts (Fig. 8g). In summary, the superiorities of SNCs on increasing metal loading, breaking linear scaling relationships, and enhancing electronic structures enable them to exhibit exceptional performance in catalysis.

DACs

The DACs have been extensively investigated as a basic and prominent category of various SNCs, combining the advantages of SACs and SNCs [173–175]. Remarkable breakthroughs have been achieved in synthesizing DACs with high metal loadings. For instance, carbon nanofibers treated with nitrogen plasma yield active sites capable of hosting Fe and Co dual atoms (Fe, Co SAs-PNCF) with a metal loading of up to 9.8 wt% (Fig. 9a) [176]. The metal loading of Fe, Co SAs-PNCF exhibits a linear correlation with the degree of defects, verifying that a higher defect density leads to a higher metal loading (Fig. 9b). Theoretically designed DACs have achieved metal loading exceeding 40 wt% by reducing the number of carbon atoms surrounding the dual-metal active sites, validating the feasibility of creating DACs with exceptionally high metal loading [177]. The significance of unique electronic structures remains pivotal in investigations concerning DACs. An example is FeCo dual atoms dispersed on an N-doped graphitic carbon (FeCo-DACs/NC), providing an avenue for designing DACs with tailored electronic structures [178]. The balance between the rate-determining steps of the oxygen electrocatalysis processes is achieved by the electron cooperation between Fe and Co atoms because the adsorption energy of intermediates is optimized by the change of the d-band. As a result, FeCo-DACs/NC exhibits superior catalytic performance in ORR, attaining a kinetic current density of up to 11.05 mA cm^{-2}.

The synergistic effect is considered a crucial feature in optimizing the catalytic performance of DACs. For instance, IrMo dual atoms on TiO_2 (Ir_1Mo_1/TiO_2 DAC) exhibit exceptional catalytic selectivity (>96% at 100% conversion) for the hydrogenation of 4-nitrostyrene (4-NS) to 4-vinylaniline [179]. This remarkable performance can be attributed to the cooperative interaction between Ir and Mo atoms in hydrogen activation and

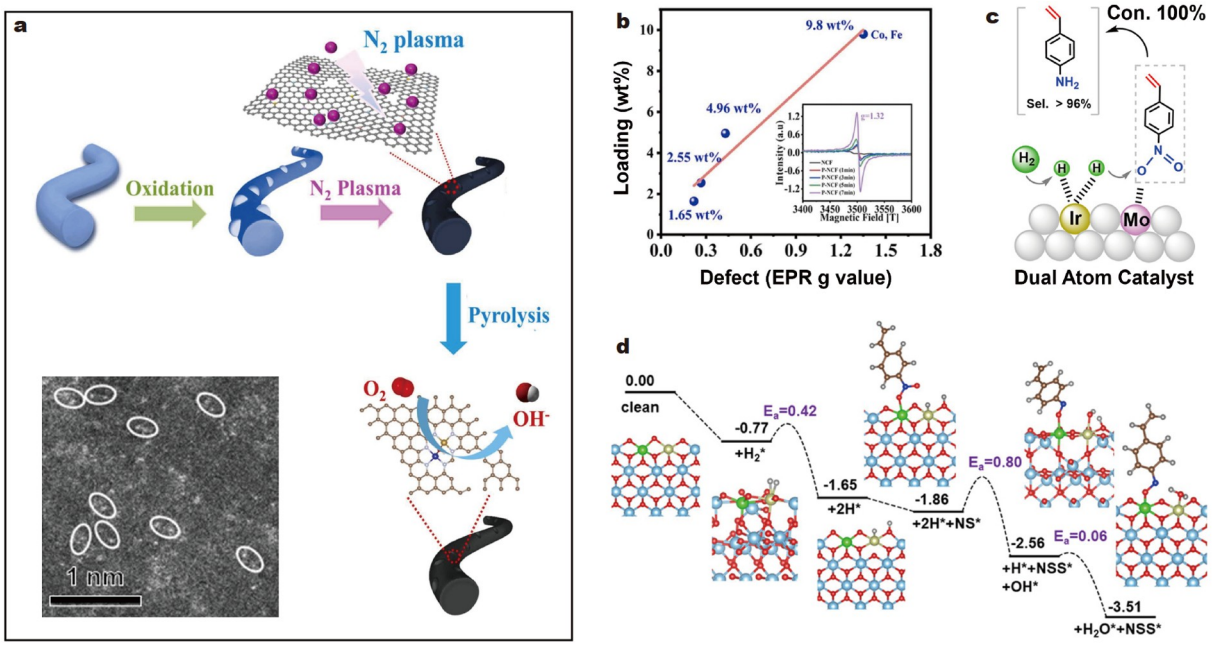

Figure 9 (a) Schematic of the preparation process of Fe, Co SAs-PNCF, and its high-angle ADF (HAADF)-STEM image. (b) Relation among the nitrogen content of Fe, Co SAs-PNCF, and the plasma treatment time. Reprinted with permission from Ref. [176]. Copyright 2022, Elsevier. (c) Schematic of the reaction pathway for Ir_1Mo_1/TiO_2 DAC, showing the cooperation between Ir and Mo atoms. (d) Energy profiles of the deoxygenation of 4-NS to 4-vinylaniline on Ir_1Mo_1/TiO_2 DAC. Unit: eV. Reprinted with permission from Ref. [179]. Copyright 2021, American Chemical Society.

4-NS adsorption (Fig. 9c). During the reaction, the total energy of the system is first decreased to −1.65 eV as Ir sites facilitate the activation of hydrogen, followed by a further reduction to −1.86 eV through the subsequent adsorption of 4-NS on Mo sites (Fig. 9d). By contrast, Ir_1/TiO_2 exhibits 38% activity at 87% conversion, and its Mo_1/TiO_2 counterpart shows no activity. A previous report explores the synergistic effect of Ag and Cu in methane oxidation [180]. The ZSM-5 supported Ag and Cu dual atoms (Ag_1-Cu_1/ZSM-5) activate the C–H bond of CH_4 and the O–O bond of H_2O_2 during the reaction. This cooperative effect leads to a selectivity of 81% while outperforming several noble metal catalysts in terms of productivity. Notably, this synergistic phenomenon is absent in Cu and Ag nanoparticles, and Ag SAC exhibits only half the productivity of Ag_1-Cu_1/ZSM-5. For homonuclear DACs, the synergistic effect is also essential. Fe dual atoms captured by carbon defects (Fe_2DAC) on the covalent organic framework (COF) were synthesized by one-step carbonization [181]. The synergistic effect of dual atoms in Fe_2DAC engenders heightened adsorption of crucial intermediates, thereby outperforming the Fe SAC counterparts in ORR activity. Furthermore, DFT calculations reveal improved charge distribution near FeCu active sites in FeCu DACs, thereby enhancing the adsorption of peroxydisulfate [182].

In summary, DACs have remarkable advantages in increasing metal loading, optimizing adsorption configurations, and modulating electronic structures. Moreover, studies of DACs provide a valuable perspective for the future development of other SNCs because DACs perform as the simplest SNCs. To further enhance the catalytic performance of DACs, efforts to broaden the range of support species are necessary. Moreover, in-depth investigations on the reaction mechanism of DACs, particularly the role of each atom in an active site during a reaction, need to be conducted.

Other SNC catalysts

In addition to DACs, SNCs comprising numerous atoms have yielded exceptional catalytic performance, meriting further exploration [4,160,183]. The synergistic effects of Cu-Pt-Au SNCs (~1 nm) result in unprecedented catalytic activity for the aerobic oxidation of hydrocarbons (i.e., 1433 metal atom^{-1} h^{-1} TOF value, which is 24 times greater than that of commercial Pt catalyst) [184]. Because of their favorable structure for C–H bond activation and butene desorption, Pt_3 SNCs exhibit remarkable selectivity (99%) and excellent conversion (35%) toward *n*-butane direct dehydrogenation [185]. This conversion is the highest compared with that of Pt nanoparticles and Pt SACs, indicating the promising prospective of SNCs in catalysis.

Similar to DACs, the electronic structure of SNCs is vastly changed by the orbital overlap between metal atoms [186]. Moreover, the electron state of SNCs is influenced by several factors, including ligands, dopants, and nuclearity [10,187,188]. Ligand-stabilized Au SNCs exhibit distinct electronic structures in comparison with their bulk Au counterparts [189]. This discrepancy includes shifts in the d-band center, reduction in spin–orbit splitting, and narrowing of the d-band. A similar phenomenon is observed in NiFeMo SNCs, wherein introducing Mo and Fe atoms through doping leads to a shift in the d-band center. Furthermore, the effect of the evolution of the electronic structure on SNC size has been systematically explored [4,188]. Researchers have conducted comprehensive investigations into the electronic structure of Pt clusters, ranging from 12 to 1415 atoms (0.7–3.5 nm in diameter) [188]. Notably, Pt SNCs composed of 13 and 55 atoms exhibit significant gaps in DOS that exert a significant influence on binding strength, which is less

pronounced in Pt clusters with more atoms. As the SNC size increases, the influence of adsorbates on charge density by adsorbates becomes more localized and finally converged to the bulk limit at 1.6 nm when the electronic finite-size effects vanish. Accordingly, Pt clusters comprising more than 147 atoms (1.7 nm) exhibit a charge density resembling that of a surface slab. This tunable electronic structure endows SNCs with catalytic performance connected with their microenvironment, particularly their constituent atom count.

Given that the catalytic performance of SNCs varies with nuclearity, a comparative investigation of the influence of nuclearity and the identification of the optimal atom count is crucial for SNC studies [190,191]. Li *et al.* [191] investigated the catalytic performance of Mo_x (x = 1–4) anchored on graphdiyne (Mo_x@GDY) for N_2RR. Mo_3@GDY with triple Mo atoms in one active site shows the best activity and selectivity for N_2RR among various samples, indicating a substantial opportunity for catalysts with triple atoms. Triple-atom catalysts also exhibit exceptional performance in other catalytic reactions. In the context of the hydrogenation of functionalized alkynes, Pd SAs, dimers, and trimers show distinct behaviors [192]. Pd trimers exhibit heightened activity because of the reduction in the hydrogen activation barrier, whereas Pd SAs exhibit enhanced selectivity and durability. Ru_3 SNCs stabilized by nitrogen species (abbreviated as Ru_3/CN) exhibit a higher TOF (4320 h^{-1}) and conversion (100%) than Ru_1/CN SAC (TOF value of 416 h^{-1} and conversion of 21%), achieving impressive activity in the selective oxidation of primary alcohols to aldehydes [193]. The excellent catalytic performance of Ru_3/CN can be attributed to its unique adsorption configuration, wherein one Ru atom is bonded with hydroxyl and amino groups. For SNCs with more atoms, the influences of nuclearity are also inevitable. Notably, SNC with 12 Pt atoms (Pt_{12} SNC) formed by the removal of an SA from the 13-atom counterpart (Pt_{13} SNC) yields a substantial enhancement of ORR activity [194]. This profound transformation is caused by the correspondence between the nuclearity of SNCs and their coordination. Specifically, Pt_{12} SNC exhibits distorted coordination, whereas Pt_{13} SNC maintains a stable icosahedral atomic arrangement.

Given the remarkable catalytic performance attained by SNCs with a specific nuclearity, the atomically precise control of the nuclearity and composition of SNCs is essential. The electronic band structure, activity, and selectivity of SNCs would be significantly changed by removing or adding an atom, enabling the effective control of the nuclearity of SNCs [195,196]. Strengthened MSI and facilitated synergistic effect could be achieved using appropriate atomic species and proportions, which enable the fine modulation of SNC composition [197–199]. For instance, different numbers of Pd atoms lead to distinct stability of the valence shell, thereby influencing the CO oxidation activity of Pd SNCs [200]. A crucial requirement for tailoring the nuclearity of SNCs is identified in Ag catalysts, where the constraints imposed by the low d-band center on their ORR performance are avoided by rationally modulated size [169]. Specifically, adatoms in Ag SNCs with 1.7 nm in size effectively induce alterations in the electronic structure, consequently enhancing the d-band center. As a result, this Ag SNC exhibits a superior 148-fold surge in mass activity of ORR compared with that of Ag nanoparticles. Based on this circumstance, the ORR performance of Ag SNCs can be optimized by atomically precise control of nuclearity. A previous study of SNCs with diverse Pd–Ru proportions reported that the naphthalene hydrogenation selectivity of Cu_6Ru_6 is higher than that of Cu_4Ru_{12}, which highlights the importance of atomically precise SNC composition [201]. To realize the atomically precise regulation of the nuclearity and composition of SNCs, considerable efforts have been made to improve their preparation methods, such as sequential self-limiting growth, deposition of defined precursors, and gas phase redispersion [202,203]. Computational research further bridges the gap between the structure and catalytic performance of SNCs [204,205]. The atomically precise modulation of the nuclearity and composition of SNCs is expected to have more exceptional outcomes in the future.

Apart from nuclearity and composition, supports also have considerable influence on the catalytic performance of SNCs, similar to that of SACs. The surface properties of supports influence not only the adsorption and dispersion of precursors but also the stability of SNCs [206,207]. The functionalization of supports further enhances their effects on SNCs. For instance, the tannic acid monolayer facilitates the adsorption of Pt precursor on carbon supports, thus enabling Pt SNCs (average diameter: ~0.4 nm) to disperse on the tannic acid monolayer-functionalized carbon surface with high density [208]. These as-prepared Pt SNCs exhibit remarkable mass activity/TOF value, surpassing that of commercial Pt/C catalysts.

As a cross-dimensional extension of ultimate structures in the scale of SAs, SNCs exhibit a satisfactory perspective for improving catalytic performance from different perspectives. The presence of additional atoms in active sites triggers a synergistic effect among metal atoms, with substantial potential for increasing metal loading, breaking linear relationships, and optimizing electronic structures. The correlation between the number of constituent atoms in SNCs and their catalytic properties provides novel insights into tailoring catalysts to meet specific demands. Moreover, the variable catalytic performance of SNCs verifies the advantages of ultimate structures in catalysis. Ultimate structures in SAs and SNCs for different reactions are summarized in Table 1 according to previous discussions, providing a comprehensive understanding of these catalysts.

ULTIMATE STRUCTURE III: ELECTRONS

Although electrons are an interior constituent of atoms, their indispensable role in modulating catalytic performance, particularly in catalysis from a microscopic perspective, has been recognized. The capacity of electrons to initiate catalytic cycles, modulate the energy barriers, and fine-tune optimized catalytic configurations enables their exploration as a unique component in catalysis. Therefore, electrons need to be considered a special category of ultimate structures in catalysis.

Among various ultimate structures that effectively modulate performance in catalysis, the smallest is an electron. The size of an electron (0.55 mg mol^{-1}) is even smaller than that of a proton (1.0 mg mol^{-1}), not to mention other atoms or SNCs [14,209]. Despite its minuscule size, the influence of electrons on catalysis is undeniable. The electron has been recognized as an effective unit in catalysis as it initiates the catalytic cycle of redox reactions [210]. A typical electron-catalyzed Diels–Alder reaction is shown in Fig. 10a, in which the electron commences the catalytic cycle [14]. A complete catalytic cycle can be achieved through the injection of electrons into substrates, the formation of intermediates, the conversion into products, and the subsequent return of electrons [14]. In-depth investigations into the role of

Table 1 Diverse ultimate structures for different reactions

Ultimate structure		Support	Reaction type	Ref.
SAC	Fe	NSFC	ORR	[50]
	Ir	Carbon nitride	CO_2RR	[58]
	Co	Graphene	HER	[60]
	Co	3D hybrid MOF	ORR	[78]
	Fe	Porous carbon	ORR/OER	[89]
	Cu	Au	Nitrate reduction reaction	[96]
	Pd	CeO_2	CO oxidation	[102]
SMAC	Ag	HMO	HCHO oxidation	[7]
SAL	Pt	SiO_2	HER	[8]
SNC	Fe, Co	PNCF	ORR	[176]
	Fe_2	COF	ORR	[181]
	Mo_x (x = 1–4)	GDY	N_2RR	[191]
	Pt_{12}	Without support	ORR	[194]

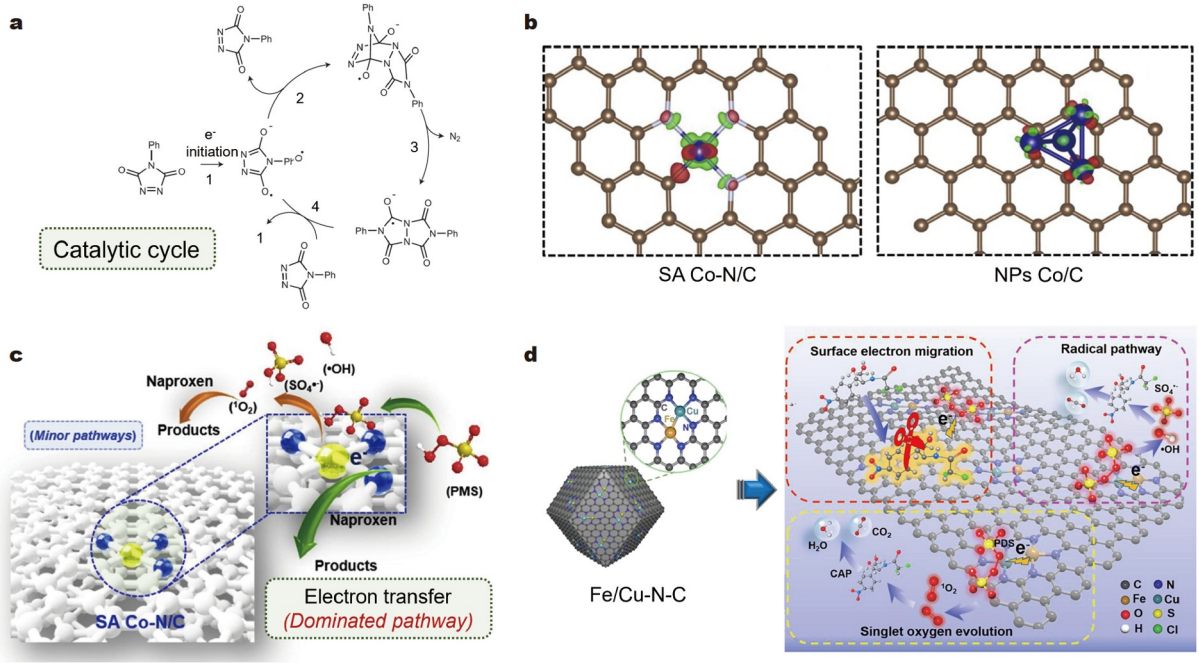

Figure 10 (a) Electron-catalyzed Diels–Alder reaction. Reprinted with permission from Ref. [14]. Copyright 2014, Springer Nature. (b) Top view of different charge densities in SA Co-N/C and NPs Co/C. (c) Catalytic mechanism of SA Co-N/C for PMS activation. Reprinted with permission from Ref. [213]. Copyright 2021, Elsevier. (d) Mechanism diagram of chloramphenicol decomposition by Fe/Cu-N-C. Reprinted with permission from Ref. [214]. Copyright 2021, Elsevier.

electrons in catalysis are frequently conducted in fields of synthetic covalent and noncovalent chemistry. For instance, introducing a chemical electron source was observed to expedite molecular recognition during the formation of a tri-radical complex, which was a kinetically prohibited process under standard conditions [211]. By applying catalytic amounts of charge, the Newman–Kwart rearrangement was observed to occur at ambient temperature, avoiding the requirement of conducting this rearrangement between 200 and 300°C [212].

More importantly, electrons represent a fundamental element that profoundly influences the catalytic performance of various catalysts, particularly those with ultimate structures. Although extensive research has focused on atoms as the fundamental components driving the improvement of catalysts with ultimate structures, the behavior of electrons determines the mechanisms of these catalysts. For instance, single Co atoms anchored on NC (denoted as SA Co-N/C) trigger the migration of electrons from peroxymonosulfate (PMS) to Co sites, resulting in the creation of electron-rich active sites surrounding the Co atoms (Fig. 10b) [213]. Conversely, in the case of nanoparticle-based Co catalyst (NPs Co/C), electron transfer occurs from Co atoms to the adjacent carbon atoms because of the interactions between the NPs Co and carbon network. In the degradation of naproxen (NPX) through PMS activation, PMS is initially adsorbed

around Co active sites. The electron-rich environment in SA Co-N/C facilitates the transfer of electrons from PMS to Co, thereby expediting NPX degradation through this electron transfer process (Fig. 10c). This electron-driven mechanism predominantly governs NPX degradation and consequently contributes to the remarkable catalytic activity (0.241 min^{-1}) of SA Co-N/C. Moreover, Cu and Ni dual atoms dispersed on N-doped carbon (abbreviated as Cu/Ni-NC) exhibit an NH_3 Faradaic efficiency of up to 97.28% during NH_3 synthesis from NO_3^- [215]. The accelerated electron transfer from Cu and Ni dual atoms to NO_3^- is a pivotal factor in enhancing the catalytic performance of Cu/Ni-NC, which is caused by the robust covalent character of Cu-Ni sites. In the case of FeCu dual atoms on nitrogen–carbon (Fe/Cu-N-C), electron transfer from Cu atoms to Fe atoms optimizes the bonding orbital distribution of Fe 3d orbitals, providing Fe atoms with a low valence state [214]. This electron-rich environment leads to the reduced adsorption energy of peroxydisulfate, enhancing its adsorption and catalytic activity in chloramphenicol decomposition. Furthermore, the electron transfer from the Fe/Cu-N-C center to peroxydisulfate facilitates the cleavage of –O–O– bonds, a critical step in the catalytic mechanism of chloramphenicol decomposition (Fig. 10d). Consequently, the removal rate of chloramphenicol increases from 0.073 to 0.093 min^{-1} compared with that of Fe SAC. Notably, the exceptional catalytic activity of colloidal Ag SNCs in the reduction of phenosafranin is attributed to their size (20–30 nm), which is suitable for efficient electron transfer [216]. The cluster potential associated with the SNC size in these Ag SNCs resides between that of the donor and acceptor, enabling Ag SNCs to function as electron relay points. The unique electron transfer pathway through Ag SNCs provides a reduced activation energy, accelerating the redox reaction. Although studies on SALs and SMACs are limited, electrons still play a significant role in research [147,217].

In summary, electrons play a modulatory role in catalysis by establishing active sites, optimizing adsorption configurations, and reducing energy barriers. These diverse influences are conducive to tailoring catalysts toward the attainment of exceptional performance. The electronic structures discussed in previous chapters also originate from the intricate behavior of electrons, further establishing electrons as a pivotal component for modulating catalysts. Furthermore, electrons function as the connective thread connect diverse ultimate structures in catalysis, thereby furnishing an invaluable avenue for the prospective advancement of catalysts.

CONCLUSION AND PERSPECTIVES

Ultimate structures, including SAs, SNCs, and electrons, have shown outstanding catalytic performance. The SAs have presented enhanced atomic use efficiency, increased specific surface area, and unsaturated coordination environments. For SNCs, the synergistic interaction between metal atoms becomes evident, enabling them to increase metal loading, disrupt linear relationships, and adjust electron configurations. The significance of electrons as the smallest category of ultimate structures has gained considerable attention, with a promising potential to provide novel insights into catalysis. However, current studies of ultimate structures in catalysis are incomprehensive. The following crucial aspects require to be explored to completely harness the potential of ultimate structures in catalysis.

(1) The integration of diverse ultimate structures in catalysts can generate further advancements in catalysis. The interactions between various ultimate structures with distinctive advantages have exhibited the potential to improve catalytic performance. For instance, the manipulation of the electronic structure of individual Fe atoms through neighboring Fe SNCs yields heightened ORR activity and improved antioxidation stability [218]. Hence, the rational combination of ultimate structures at different scales emerges as a viable strategy to improve catalytic performance.

(2) Emphasizing the stability of catalysts with ultimate structures is imperative for enhancing catalytic performance. The tendency for aggregation inherent in ultimate structures exhibits the necessity for robust stability during chemical reactions. Numerous investigations have made efforts to improve the stability of ultimate structures in catalysis, in which the pivotal points are exploiting adjacent atoms or defects and promoting the interactions between ultimate structures and supports. [35,219,220]. Dopants, vacancies, and edges on support surfaces are frequently exploited to regulate the microenvironment of ultimate structures precisely, thus enhancing their catalytic stability. Supports with highly electronegative atoms could also anchor and stabilize ultimate structures by strengthening their bond. Notably, strong MSI enables Pt SAs to disperse on α-Fe_2O_3 stably, even without surface defects. Encapsulation and appropriate preparation methods, including coprecipitation and pyrolysis, for stable ultimate structures have also been evaluated in previous studies [30,221,222]. Moreover, ultimate structures with well-designed geometric features to separate SAs or SNCs can effectively enhance their stability. An example is Pt SAs that are confined by oxide SNCs and unable to move across clusters [219]. These obtained Pt SAs maintain atomic dispersion under oxidizing and reducing environments, which is beneficial for practical applications. In the future, in-depth research on stabilizing catalysts with ultimate structures in diverse environments will further exert substantial influence on catalysis.

(3) Controllable synthesis is important for the industrial usage of catalysts with ultimate structures. The catalytic performance of catalysts is substantially dependent on their structural features, including factors such as metal loading, atomic distribution, and electronic structure. However, maintaining precise ultimate structures, particularly the well-designed distribution of SAs, is a challenge during the preparation of catalysts. Several strategies have been exploited to address this issue. Strengthened MSI not only contributes to the formation and stability of ultimate structures but also enables them to retain their features during preparation. Methods involving the functionalization of supports or precursors and defect engineering have been verified to be effective [128,223,224]. The appropriate selection of preparation methods helps maintain ultimate structures. Rapid thermal treatment has a remarkable effect on maintaining the dispersion of SAs, which is difficult for conventional preparation methods to achieve [128]. Recently, the unique arrangement of atoms by spatial confinements has emerged as a powerful approach to stabilizing ultimate structures because it could prevent the disassembly and aggregation of ultimate structures. An example of this strategy is Pt SAs and SNCs prepared by the confinement of cups and cages in zeolites [225]. Comprehensive research on the controllable synthesis of ultimate structures is required, considering that the tradeoff between controllable synthesis and cost efficiency persists even for extensively investigated SACs. Therefore, attaining breakthroughs in syn-

thesizing catalysts with controllable ultimate structures will contribute to their large-scale applications.

(4) The manipulation of electron transfer is crucial for investigating ultimate structures in catalysis. Electrons play a significant role in optimizing adsorption configurations and rationalizing reaction pathways, which makes it imperative to improve catalytic performance through well-tuned electron transfer within reactions. Therefore, for ultimate structures in future catalysis, efforts to achieve well-designed control of electron transfer mechanisms become indispensable. Representative strategies to address this issue involve surface modification, heterojunction constructions, and configuration modification. The introduction of dopants, vacancies, and ligands to supports has been extensively used to tune the charge transfer in ultimate structures. Recently, heterojunctions expediting the efficient separation and fast transportation of charge carriers have received increasing attention and serve as a powerful approach to enhancing catalytic performance by designing electron transfer mechanisms [226–228]. Moreover, the asymmetry of atomic configurations could be used to regulate charge distribution, particularly for that in SNCs [159,229]. For future developments of ultimate structures in catalysis, strategies to realize controllable and well-designed electron transfer mechanisms would be valued.

(5) The development of techniques for precise characterization and identification could provide effective information on the structure and evolution of SAs. Techniques to characterize SAs, such as X-ray absorption spectroscopy, scanning tunneling microscopy, and TEM, have also received increasing attention. With improvements in synthesizing SAs with ultimate structures for catalysis, further studies should be directed to dynamic and *in situ* characterization techniques, which could reveal the behavior of SAs under reactions. Considering the limitation of extended X-ray absorption fine structure (EXAFS) to distinguish SAs and clusters, precise and comprehensive identification techniques of diverse ultimate structures are also merited [230].

Received 1 September 2023; accepted 6 November 2023; published online 28 November 2023

1 Yang XF, Wang A, Qiao B, *et al.* Single-atom catalysts: A new frontier in heterogeneous catalysis. Acc Chem Res, 2013, 46: 1740–1748
2 Singh B, Sharma V, Gaikwad RP, *et al.* Single-atom catalysts: A sustainable pathway for the advanced catalytic applications. Small, 2021, 17: 2006473
3 Fonseca J, Lu J. Single-atom catalysts designed and prepared by the atomic layer deposition technique. ACS Catal, 2021, 11: 7018–7059
4 Sharma S, Ansari A. Metal and metal oxide sub nano cluster; emerging aspirant for catalytic applications. Results Chem, 2023, 5: 100982
5 Chu T, Rong C, Zhou L, *et al.* Progress and perspectives of single-atom catalysts for gas sensing. Adv Mater, 2022, 35: 2206783
6 Qiao B, Wang A, Yang X, *et al.* Single-atom catalysis of CO oxidation using Pt_1/FeO_x. Nat Chem, 2011, 3: 634–641
7 Huang Z, Gu X, Cao Q, *et al.* Catalytically active single-atom sites fabricated from silver particles. Angew Chem Int Ed, 2012, 51: 4198–4203
8 He Y, Liu L, Zhu C, *et al.* Amorphizing noble metal chalcogenide catalysts at the single-layer limit towards hydrogen production. Nat Catal, 2022, 5: 212–221
9 Ma M, Gong C, An X, *et al.* The emergence of single-atom-layer catalysis. Mater Today Catal, 2023, 1: 100004
10 Sun L, Reddu V, Wang X. Multi-atom cluster catalysts for efficient electrocatalysis. Chem Soc Rev, 2022, 51: 8923–8956
11 Li R, Wang D. Superiority of dual-atom catalysts in electrocatalysis: One step further than single-atom catalysts. Adv Energy Mater, 2022, 12: 2103564
12 Chen ZW, Chen LX, Yang CC, *et al.* Atomic (single, double, and triple atoms) catalysis: Frontiers, opportunities, and challenges. J Mater Chem A, 2019, 7: 3492–3515
13 Nguyen DT, Do TO. Comprehensive review for an efficient charge transfer in single atomic site catalyst/organic polymers toward photocatalytic CO_2 reduction. Adv Mater Inter, 2023, 10: 2201413
14 Studer A, Curran DP. The electron is a catalyst. Nat Chem, 2014, 6: 765–773
15 Guo S, Fu J, Zhang P, *et al.* Direct growth of single-metal-atom chains. Nat Synth, 2022, 1: 245–253
16 Li Y, He Z, Wu F, *et al.* Defect engineering of high-loading single-atom catalysts for electrochemical carbon dioxide reduction. Mater Rep-Energy, 2023, 3: 100197
17 Shen T, Wang S, Zhao T, *et al.* Recent advances of single-atom-alloy for energy electrocatalysis. Adv Energy Mater, 2022, 12: 2201823
18 Rao P, Wu D, Qin YY, *et al.* Facile fabrication of single-atom catalysts by a plasma-etching strategy for oxygen reduction reaction. J Mater Chem A, 2022, 10: 6531–6537
19 Zeng L, Xue C. Single metal atom decorated photocatalysts: Progress and challenges. Nano Res, 2020, 14: 934–944
20 Zhang H, Liu G, Shi L, *et al.* Single-atom catalysts: Emerging multifunctional materials in heterogeneous catalysis. Adv Energy Mater, 2018, 8:
21 Iqbal MS, Yao ZB, Ruan YK, *et al.* Single-atom catalysts for electrochemical N_2 reduction to NH_3. Rare Met, 2023, 42: 1075–1097
22 Xue ZH, Luan D, Zhang H, *et al.* Single-atom catalysts for photocatalytic energy conversion. Joule, 2022, 6: 92–133
23 Qin R, Liu K, Wu Q, *et al.* Surface coordination chemistry of atomically dispersed metal catalysts. Chem Rev, 2020, 120: 11810–11899
24 Wang A, Li J, Zhang T. Heterogeneous single-atom catalysis. Nat Rev Chem, 2018, 2: 65–81
25 Chen Y, Wang L, Yao Z, *et al.* Tuning the coordination structure of single atoms and their interaction with the support for carbon dioxide electroreduction. Acta Physico Chim Sin, 2022, 0: 2207024–0
26 Li J, Banis MN, Ren Z, *et al.* Unveiling the nature of Pt single-atom catalyst during electrocatalytic hydrogen evolution and oxygen reduction reactions. Small, 2021, 17: 2007245
27 Choi CH, Kim M, Kwon HC, *et al.* Tuning selectivity of electrochemical reactions by atomically dispersed platinum catalyst. Nat Commun, 2016, 7: 10922
28 Gao G, Jiao Y, Waclawik ER, *et al.* Single atom (Pd/Pt) supported on graphitic carbon nitride as an efficient photocatalyst for visible-light reduction of carbon dioxide. J Am Chem Soc, 2016, 138: 6292–6297
29 Zhu C, Fu S, Shi Q, *et al.* Single-atom electrocatalysts. Angew Chem Int Ed, 2017, 56: 13944–13960
30 Xiong H, Datye AK, Wang Y. Thermally stable single-atom heterogeneous catalysts. Adv Mater, 2021, 33: 2004319
31 Wei H, Liu X, Wang A, *et al.* FeO_x-supported platinum single-atom and pseudo-single-atom catalysts for chemoselective hydrogenation of functionalized nitroarenes. Nat Commun, 2014, 5: 5634
32 Zhang H, Zuo S, Qiu M, *et al.* Direct probing of atomically dispersed Ru species over multi-edged TiO_2 for highly efficient photocatalytic hydrogen evolution. Sci Adv, 2020, 6: eabb9823
33 Bulushev DA, Nishchakova AD, Trubina SV, *et al.* Ni-N_4 sites in a single-atom Ni catalyst on N-doped carbon for hydrogen production from formic acid. J Catal, 2021, 402: 264–274
34 Wang K, Wang X, Liang X. Synthesis of high metal loading single atom catalysts and exploration of the active center structure. ChemCatChem, 2020, 13: 28–58
35 Kaiser SK, Fako E, Manzocchi G, *et al.* Nanostructuring unlocks high performance of platinum single-atom catalysts for stable vinyl chloride production. Nat Catal, 2020, 3: 376–385
36 Wang L, Zhao X, Yang X, *et al.* Thermally stable single atom catalysts: From concept to *in situ* study. Funct Mater Lett, 2021, 14: 2130007
37 Zhang J, Zhao Y, Chen C, *et al.* Tuning the coordination environment in single-atom catalysts to achieve highly efficient oxygen reduction

reactions. J Am Chem Soc, 2019, 141: 20118–20126
38 Xu H, Zhao Y, Wang Q, *et al.* Supports promote single-atom catalysts toward advanced electrocatalysis. Coord Chem Rev, 2022, 451: 214261
39 Park J, Lee S, Kim HE, *et al.* Investigation of the support effect in atomically dispersed Pt on WO_{3-x} for utilization of Pt in the hydrogen evolution reaction. Angew Chem Int Ed, 2019, 58: 16038–16042
40 Zhang B, Asakura H, Zhang J, *et al.* Stabilizing a platinum$_1$ single-atom catalyst on supported phosphomolybdic acid without compromising hydrogenation activity. Angew Chem Int Ed, 2016, 55: 8319–8323
41 Liu Z, Li S, Yang J, *et al.* Ultrafast construction of oxygen-containing scaffold over graphite for trapping Ni^{2+} into single atom catalysts. ACS Nano, 2020, 14: 11662–11669
42 Zhang J, Yang H, Liu B. Coordination engineering of single-atom catalysts for the oxygen reduction reaction: A review. Adv Energy Mater, 2020, 11: 2002473
43 Zhang X, Guo J, Guan P, *et al.* Catalytically active single-atom niobium in graphitic layers. Nat Commun, 2013, 4: 1924
44 Lai WH, Miao Z, Wang YX, *et al.* Atomic-local environments of single-atom catalysts: Synthesis, electronic structure, and activity. Adv Energy Mater, 2019, 9:
45 Lou Y, Liu J. CO oxidation on metal oxide supported single Pt atoms: The role of the support. Ind Eng Chem Res, 2017, 56: 6916–6925
46 Zhang Y, Guo L, Tao L, *et al.* Defect-based single-atom electrocatalysts. Small Methods, 2019, 3:
47 Baby A, Trovato L, Di Valentin C. Single atom catalysts (SAC) trapped in defective and nitrogen-doped graphene supported on metal substrates. Carbon, 2021, 174: 772–788
48 Bakandritsos A, Kadam RG, Kumar P, *et al.* Single-atom catalysis: Mixed-valence single-atom catalyst derived from functionalized graphene. Adv Mater, 2019, 31:
49 Gawande MB, Fornasiero P, Zbořil R. Carbon-based single-atom catalysts for advanced applications. ACS Catal, 2020, 10: 2231–2259
50 Zhou Y, Tao X, Chen G, *et al.* Multilayer stabilization for fabricating high-loading single-atom catalysts. Nat Commun, 2020, 11: 5892
51 Zhang S, Ao X, Huang J, *et al.* Isolated single-atom Ni–N_5 catalytic site in hollow porous carbon capsules for efficient lithium–sulfur batteries. Nano Lett, 2021, 21: 9691–9698
52 Zuo Y, Li T, Zhang N, *et al.* Spatially confined formation of single atoms in highly porous carbon nitride nanoreactors. ACS Nano, 2021, 15: 7790–7798
53 Guo J, Huo J, Liu Y, *et al.* Nitrogen-doped porous carbon supported nonprecious metal single-atom electrocatalysts: From synthesis to application. Small Methods, 2019, 3:
54 Han Y, Duan H, Liu W, *et al.* Engineering the electronic structure of platinum single-atom sites *via* tailored porous carbon nanofibers for large-scale hydrogen production. Appl Catal B-Environ, 2023, 335: 122898
55 Chen Y, Zou L, Liu H, *et al.* Fe and N co-doped porous carbon nanospheres with high density of active sites for efficient CO_2 electroreduction. J Phys Chem C, 2019, 123: 16651–16659
56 Li M, Wang H, Luo W, *et al.* Heterogeneous single-atom catalysts for electrochemical CO_2 reduction reaction. Adv Mater, 2020, 32: 2001848
57 Han L, Liu X, Chen J, *et al.* Atomically dispersed molybdenum catalysts for efficient ambient nitrogen fixation. Angew Chem Int Ed, 2019, 58: 2321–2325
58 Sharma P, Kumar S, Tomanec O, *et al.* Carbon nitride-based ruthenium single atom photocatalyst for CO_2 reduction to methanol. Small, 2021, 17: 2006478
59 Feng Q, Zhao S, Xu Q, *et al.* Mesoporous nitrogen-doped carbon-nanosphere-supported isolated single-atom Pd catalyst for highly efficient semihydrogenation of acetylene. Adv Mater, 2019, 31:
60 Huang K, Wei Z, Liu J, *et al.* Engineering the morphology and microenvironment of a graphene-supported Co-N-C single-atom electrocatalyst for enhanced hydrogen evolution. Small, 2022, 18: 2201139
61 Sui J, Liu H, Hu S, *et al.* A general strategy to immobilize single-atom catalysts in metal-organic frameworks for enhanced photocatalysis. Adv Mater, 2022, 34: 2109203
62 Yang X, Wang J, Wei Y, *et al.* Cotton-derived carbon fiber-supported Ni nanoparticles as nanoislands to anchor single-atom Pt for efficient catalytic reduction of 4-nitrophenol. Appl Catal A-Gen, 2022, 643: 118734
63 Hasani A, Teklagne MA, Do HH, *et al.* Graphene-based catalysts for electrochemical carbon dioxide reduction. Carbon Energy, 2020, 2: 158–175
64 Zhuo HY, Zhang X, Liang JX, *et al.* Theoretical understandings of graphene-based metal single-atom catalysts: Stability and catalytic performance. Chem Rev, 2020, 120: 12315–12341
65 Yam K, Guo N, Jiang Z, *et al.* Graphene-based heterogeneous catalysis: Role of graphene. Catalysts, 2020, 10: 53
66 Kim TY, Park CH, Marzari N. The electronic thermal conductivity of graphene. Nano Lett, 2016, 16: 2439–2443
67 Huang H, Yan M, Yang C, *et al.* Graphene nanoarchitectonics: Recent advances in graphene-based electrocatalysts for hydrogen evolution reaction. Adv Mater, 2019, 31:
68 Geim AK. Graphene: Status and prospects. Science, 2009, 324: 1530–1534
69 Zhang Q, Zhang X, Wang J, *et al.* Graphene-supported single-atom catalysts and applications in electrocatalysis. Nanotechnology, 2021, 32: 032001
70 Hu L, Hu X, Wu X, *et al.* Density functional calculation of transition metal adatom adsorption on graphene. Physica B-Condensed Matter, 2010, 405: 3337–3341
71 Huang F, Deng Y, Chen Y, *et al.* Anchoring Cu$_1$ species over nanodiamond-graphene for semi-hydrogenation of acetylene. Nat Commun, 2019, 10: 4431
72 Li B, Wen HM, Cui Y, *et al.* Emerging multifunctional metal-organic framework materials. Adv Mater, 2016, 28: 8819–8860
73 Jiao L, Wang Y, Jiang HL, *et al.* Metal-organic frameworks as platforms for catalytic applications. Adv Mater, 2018, 30:
74 Han A, Wang B, Kumar A, *et al.* Recent advances for MOF-derived carbon-supported single-atom catalysts. Small Methods, 2019, 3:
75 Zuo Q, Liu T, Chen C, *et al.* Ultrathin metal-organic framework nanosheets with ultrahigh loading of single Pt atoms for efficient visible-light-driven photocatalytic H_2 evolution. Angew Chem Int Ed, 2019, 58: 10198–10203
76 Jiao L, Jiang HL. Metal-organic-framework-based single-atom catalysts for energy applications. Chem, 2019, 5: 786–804
77 Xia P, Wang C, He Q, *et al.* MOF-derived single-atom catalysts: The next frontier in advanced oxidation for water treatment. Chem Eng J, 2023, 452: 139446
78 Zhou L, Zhou P, Zhang Y, *et al.* 3D star-like atypical hybrid MOF derived single-atom catalyst boosts oxygen reduction catalysis. J Energy Chem, 2021, 55: 355–360
79 Hao YC, Chen LW, Li J, *et al.* Metal-organic framework membranes with single-atomic centers for photocatalytic CO_2 and O_2 reduction. Nat Commun, 2021, 12: 2682
80 Xiao J, Zhang T, Wang Q. Metal-organic framework derived single-atom catalysts for CO_2 conversion to methanol. Curr Opin Green Sustain Chem, 2022, 37: 100660
81 Rivera-Cárcamo C, Serp P. Single atom catalysts on carbon-based materials. ChemCatChem, 2018, 10: 5058–5091
82 Zhang P, Zhao Z, Dyatkin B, *et al. In situ* synthesis of cotton-derived Ni/C catalysts with controllable structures and enhanced catalytic performance. Green Chem, 2016, 18: 3594–3599
83 Wang Y, Yu B, Liu K, *et al.* Co single-atoms on ultrathin N-doped porous carbon *via* a biomass complexation strategy for high performance metal-air batteries. J Mater Chem A, 2020, 8: 2131–2139
84 Wang Y, Zhang M, Shen X, *et al.* Biomass-derived carbon materials: Controllable preparation and versatile applications. Small, 2021, 17: 2008079
85 Shen M, Hu W, Duan C, *et al.* Cellulose nanofibers carbon aerogel based single-cobalt-atom catalyst for high-efficiency oxygen reduction and zinc-air battery. J Colloid Interface Sci, 2023, 629: 778–785
86 Liu Y, Zhou H, Jin C, *et al.* Bio-porphyrin supported single-atom iron catalyst boosting peroxymonosulfate activation for pollutants degradation: A singlet oxygen-dominated nonradical pathway. Appl Catal B-Environ, 2023, 338: 123061

87 Wang X, Du J, Zhang Q, *et al.* *In situ* synthesis of sustainable highly efficient single iron atoms anchored on nitrogen doped carbon derived from renewable biomass. Carbon, 2020, 157: 614–621
88 Lee DW, Jang JH, Jang I, *et al.* Bio-derived Co_2P nanoparticles supported on nitrogen-doped carbon as promising oxygen reduction reaction electrocatalyst for anion exchange membrane fuel cells. Small, 2019, 15:
89 Zhong L, Jiang C, Zheng M, *et al.* Wood carbon based single-atom catalyst for rechargeable Zn-air batteries. ACS Energy Lett, 2021, 6: 3624–3633
90 Yang F, Xu W. Synergistically enhanced single-atomic site catalysts for clean energy conversion. J Mater Chem A, 2022, 10: 5673–5698
91 Yu Y, Dong X', Chen P, *et al.* Synergistic effect of Cu single atoms and Au-Cu alloy nanoparticles on TiO_2 for efficient CO_2 photoreduction. ACS Nano, 2021, 15: 14453–14464
92 Greiner MT, Jones TE, Beeg S, *et al.* Free-atom-like d states in single-atom alloy catalysts. Nat Chem, 2018, 10: 1008–1015
93 Duchesne PN, Li ZY, Deming CP, *et al.* Golden single-atomic-site platinum electrocatalysts. Nat Mater, 2018, 17: 1033–1039
94 Spivey TD, Holewinski A. Selective interactions between free-atom-like d-states in single-atom alloy catalysts and near-frontier molecular orbitals. J Am Chem Soc, 2021, 143: 11897–11902
95 Hannagan RT, Giannakakis G, Réocreux R, *et al.* First-principles design of a single-atom–alloy propane dehydrogenation catalyst. Science, 2021, 372: 1444–1447
96 Zhang Y, Chen X, Wang W, *et al.* Electrocatalytic nitrate reduction to ammonia on defective Au_1Cu (111) single-atom alloys. Appl Catal B-Environ, 2022, 310: 121346
97 Zhao J, Liu J, Li Z, *et al.* Ruthenium-cobalt single atom alloy for CO photo-hydrogenation to liquid fuels at ambient pressures. Nat Commun, 2023, 14: 1909
98 Zhang H, Tian W, Duan X, *et al.* Single-atom catalysts on metal-based supports for solar photoreduction catalysis. Chin J Catal, 2022, 43: 2301–2315
99 Mohanty B, Basu S, Jena BK. Transition metal-based single-atom catalysts (TM-SACs); rising materials for electrochemical CO_2 reduction. J Energy Chem, 2022, 70: 444–471
100 Tian S, Gong W, Chen W, *et al.* Regulating the catalytic performance of single-atomic-site Ir catalyst for biomass conversion by metal–support interactions. ACS Catal, 2019, 9: 5223–5230
101 Han F, Zhou Z, Zhang X, *et al.* First-principles study on stability and HER activity of noble metal single atoms on TiO_2: The effect of loading density. J Phys Chem C, 2018, 122: 2546–2553
102 Muravev V, Spezzati G, Su YQ, *et al.* Interface dynamics of Pd–CeO_2 single-atom catalysts during CO oxidation. Nat Catal, 2021, 4: 469–478
103 Daelman N, Capdevila-Cortada M, López N. Dynamic charge and oxidation state of Pt/CeO_2 single-atom catalysts. Nat Mater, 2019, 18: 1215–1221
104 Liu D, He Q, Ding S, *et al.* Structural regulation and support coupling effect of single-atom catalysts for heterogeneous catalysis. Adv Energy Mater, 2020, 10: 2001482
105 Liu G, Huang Y, Lv H, *et al.* Confining single-atom Pd on g-C_3N_4 with carbon vacancies towards enhanced photocatalytic NO conversion. Appl Catal B-Environ, 2021, 284: 119683
106 Yang Q, Liu H, Yuan P, *et al.* Single carbon vacancy traps atomic platinum for hydrogen evolution catalysis. J Am Chem Soc, 2022, 144: 2171–2178
107 Rong X, Wang HJ, Lu XL, *et al.* Controlled synthesis of a vacancy-defect single-atom catalyst for boosting CO_2 electroreduction. Angew Chem Int Ed, 2020, 59: 1961–1965
108 Wan J, Chen W, Jia C, *et al.* Defect effects on TiO_2 nanosheets: Stabilizing single atomic site Au and promoting catalytic properties. Adv Mater, 2018, 30:
109 Kim IH, Lim J, Kim SO. Discovery of single-atom catalyst: Customized heteroelement dopants on graphene. Acc Mater Res, 2021, 2: 394–406
110 Liu W, Chen Y, Qi H, *et al.* A durable nickel single-atom catalyst for hydrogenation reactions and cellulose valorization under harsh conditions. Angew Chem Int Ed, 2018, 57: 7071–7075
111 Xu Q, Guo C, Li B, *et al.* Al^{3+} dopants induced Mg^{2+} vacancies stabilizing single-atom Cu catalyst for efficient free-radical hydrophosphinylation of alkenes. J Am Chem Soc, 2022, 144: 4321–4326
112 Liu W, Zhang H, Li C, *et al.* Non-noble metal single-atom catalysts prepared by wet chemical method and their applications in electrochemical water splitting. J Energy Chem, 2020, 47: 333–345
113 Fu Y, Chan YT, Jiang YP, *et al.* Polarity-differentiated dielectric materials in monolayer graphene charge-regulated field-effect transistors for an artificial reflex arc and pain-modulation system of the spinal cord. Adv Mater, 2022, 34: 2202059
114 Dvořák F, Farnesi Camellone M, Tovt A, *et al.* Creating single-atom Pt-ceria catalysts by surface step decoration. Nat Commun, 2016, 7: 10801
115 Shang H, Zhou X, Dong J, *et al.* Engineering unsymmetrically coordinated Cu-S_1N_3 single atom sites with enhanced oxygen reduction activity. Nat Commun, 2020, 11: 3049
116 Tang C, Jiao Y, Shi B, *et al.* Coordination tunes selectivity: Two-electron oxygen reduction on high-loading molybdenum single-atom catalysts. Angew Chem, 2020, 132: 9256–9261
117 Ali S, Iqbal R, Khan A, *et al.* Stability and catalytic performance of single-atom catalysts supported on doped and defective graphene for CO_2 hydrogenation to formic acid: A first-principles study. ACS Appl Nano Mater, 2021, 4: 6893–6902
118 Li J, Zhang L, Doyle-Davis K, *et al.* Recent advances and strategies in the stabilization of single-atom catalysts for electrochemical applications. Carbon Energy, 2020, 2: 488–520
119 Guo Y, Yao S, Xue Y, *et al.* Nickel single-atom catalysts intrinsically promoted by fast pyrolysis for selective electroreduction of CO_2 into CO. Appl Catal B-Environ, 2022, 304: 120997
120 Kraushofer F, Parkinson GS. Single-atom catalysis: Insights from model systems. Chem Rev, 2022, 122: 14911–14939
121 Ban J, Wen X, Xu H, *et al.* Dual evolution in defect and morphology of single-atom dispersed carbon based oxygen electrocatalyst. Adv Funct Mater, 2021, 31: 2010472
122 Hiragond CB, Powar NS, Lee J, *et al.* Single-atom catalysts (SACs) for photocatalytic CO_2 reduction with H_2O: Activity, product selectivity, stability, and surface chemistry. Small, 2022, 18: 2201428
123 Li X, Rong H, Zhang J, *et al.* Modulating the local coordination environment of single-atom catalysts for enhanced catalytic performance. Nano Res, 2020, 13: 1842–1855
124 Zhang Q, Guan J. Applications of single-atom catalysts. Nano Res, 2021, 15: 38–70
125 Tang Q, Longshuai Z, Zou J. High-loading Fe single-atom catalyst for 100% selectivity of $^1O_2$ generation. Chin Struct Chem. 2022, 41: 220800
126 Jin J, Han X, Fang Y, *et al.* Microenvironment engineering of Ru single-atom catalysts by regulating the cation vacancies in NiFe-layered double hydroxides. Adv Funct Mater, 2021, 32: 2109218
127 Wang L, Zhu C, Xu M, *et al.* Boosting activity and stability of metal single-atom catalysts *via* regulation of coordination number and local composition. J Am Chem Soc, 2021, 143: 18854–18858
128 Ren Y, Tang Y, Zhang L, *et al.* Unraveling the coordination structure-performance relationship in Pt_1/Fe_2O_3 single-atom catalyst. Nat Commun, 2019, 10: 4500
129 Song P, Zhu P, Su X, *et al.* Microenvironment modulation in carbon-supported single-atom catalysts for efficient electrocatalytic CO_2 reduction. Chem — An Asian J, 2022, 17: e202200716
130 Chi K, Wu Y, Wang X, *et al.* Single atom catalysts with out-of-plane coordination structure on conjugated covalent organic frameworks. Small, 2022, 18: 2203966
131 Omr HAE, Horn MW, Lee H. Low-dimensional nanostructured photocatalysts for efficient CO_2 conversion into solar fuels. Catalysts, 2021, 11: 418
132 Chu X, Wang K, Qian W, *et al.* Surface and interfacial engineering of 1D Pt-group nanostructures for catalysis. Coord Chem Rev, 2023, 477: 214952
133 Li C, Guo R, Wu T, *et al.* Progress and perspectives on 1D nanostructured catalysts applied in photo(electro)catalytic reduction of CO_2.

Nanoscale, 2022, 14: 16033–16064
134 Wu M, Li C, Liu R. Freestanding 1D hierarchical porous Fe-N-doped carbon nanofibers as efficient oxygen reduction catalysts for Zn-air batteries. Energy Tech, 2019, 7:
135 Ahn SH, Yu X, Manthiram A. "Wiring" Fe-N_x-embedded porous carbon framework onto 1D nanotubes for efficient oxygen reduction reaction in alkaline and acidic media. Adv Mater, 2017, 29:
136 Rubio-Bollinger G, Bahn SR, Agraït N, *et al.* Mechanical properties and formation mechanisms of a wire of single gold atoms. Phys Rev Lett, 2001, 87: 026101
137 Lee JY, Choi GH, Moon J, *et al.* 1D Co_4S_3 nanoneedle array with mesoporous carbon derived from double comb copolymer as an efficient solar conversion catalyst. Appl Surf Sci, 2021, 535: 147637
138 Wang Y, Su YR, Qiao L, *et al.* Synthesis of one-dimensional TiO_2/V_2O_5 branched heterostructures and their visible light photocatalytic activity towards Rhodamine B. Nanotechnology, 2011, 22: 225702
139 Li H, Zhang XQ, Sun FW, *et al.* Theoretical study of the electrical transport of nickel nanowires and a single atomic chain. J Appl Phys, 2007, 102: 013702
140 Ohnishi H, Kondo Y, Takayanagi K. Quantized conductance through individual rows of suspended gold atoms. Nature, 1998, 395: 780–783
141 Wang L, Wang J, Gao X, *et al.* Periodic one-dimensional single-atom arrays. J Am Chem Soc, 2022, 144: 15999–16005
142 Beniya A, Higashi S. Towards dense single-atom catalysts for future automotive applications. Nat Catal, 2019, 2: 590–602
143 Lee SH, Kwak EH, Jeong GH. Dewetting behavior of electron-beam-deposited Au thin films on various substrates: Graphenes, quartz, and SiO_2 wafers. Appl Phys A, 2014, 118: 389–396
144 Duan H, Wang C, Li G, *et al.* Single-atom-layer catalysis in a MoS_2 monolayer activated by long-range ferromagnetism for the hydrogen evolution reaction: Beyond single-atom catalysis. Angew Chem Int Ed, 2021, 60: 7251–7258
145 Saleem F, Xu B, Ni B, *et al.* Atomically thick Pt-Cu nanosheets: Self-assembled sandwich and nanoring-like structures. Adv Mater, 2015, 27: 2013–2018
146 Jiang J, Ding W, Li W, *et al.* Freestanding single-atom-layer Pd-based catalysts: Oriented splitting of energy bands for unique stability and activity. Chem, 2020, 6: 431–447
147 Jiang D, Yuan H, Liu Z, *et al.* Defect-anchored single-atom-layer Pt clusters on TiO_{2-x}/Ti for efficient hydrogen evolution *via* photothermal reforming plastics. Appl Catal B-Environ, 2023, 339: 123081
148 Duan L, Hung CT, Wang J, *et al.* Synthesis of fully exposed single-atom-layer metal clusters on 2D ordered mesoporous TiO_2 nanosheets. Angew Chem Int Ed, 2022, 61: e202211307
149 He T, Santiago ARP, Kong Y, *et al.* Atomically dispersed heteronuclear dual-atom catalysts: A new rising star in atomic catalysis. Small, 2021, 18: 2106091
150 Peterson AA, Nørskov JK. Activity descriptors for CO_2 electroreduction to methane on transition-metal catalysts. J Phys Chem Lett, 2012, 3: 251–258
151 Chen C, Sun M, Wang K, *et al.* Dual-metal single-atomic catalyst: The challenge in synthesis, characterization, and mechanistic investigation for electrocatalysis. SmartMat, 2022, 3: 533–564
152 Pérez-Ramírez J, López N. Strategies to break linear scaling relationships. Nat Catal, 2019, 2: 971–976
153 Qian H, Zhu M, Wu Z, *et al.* Quantum sized gold nanoclusters with atomic precision. Acc Chem Res, 2012, 45: 1470–1479
154 Schmid G, Bäumle M, Geerkens M, *et al.* Current and future applications of nanoclusters. Chem Soc Rev, 1999, 28: 179–185
155 Chen S, Cui M, Yin Z, *et al.* Single-atom and dual-atom electrocatalysts derived from metal organic frameworks: Current progress and perspectives. ChemSusChem, 2020, 14: 73–93
156 Andersen M, Medford AJ, Nørskov JK, *et al.* Scaling-relation-based analysis of bifunctional catalysis: The case for homogeneous bimetallic alloys. ACS Catal, 2017, 7: 3960–3967
157 Li L, Yuan K, Chen Y. Breaking the scaling relationship limit: From single-atom to dual-atom catalysts. Acc Mater Res, 2022, 3: 584–596
158 Fang C, Zhou J, Zhang L, *et al.* Synergy of dual-atom catalysts deviated from the scaling relationship for oxygen evolution reaction. Nat Commun, 2023, 14: 4449
159 Yao D, Tang C, Zhi X, *et al.* Inter-metal interaction with a threshold effect in NiCu dual-atom catalysts for CO_2 electroreduction. Adv Mater, 2023, 35: 2209386
160 Hamilton JF, Baetzold RC. Catalysis by small metal clusters. Science, 1979, 205: 1213–1220
161 Zou L, Wei YS, Hou CC, *et al.* Single-atom catalysts derived from metal-organic frameworks for electrochemical applications. Small, 2021, 17: 2004809
162 Peng M, Dong C, Gao R, *et al.* Fully exposed cluster catalyst (FECC): Toward rich surface sites and full atom utilization efficiency. ACS Cent Sci, 2020, 7: 262–273
163 Zuo Y, Wang Z, Zhao H, *et al.* Synthesis of a spatially confined, highly durable, and fully exposed Pd cluster catalyst *via* sequential site-selective atomic layer deposition. ACS Appl Mater Interfaces, 2022, 14: 14466–14473
164 Wei YS, Sun L, Wang M, *et al.* Fabricating dual-atom iron catalysts for efficient oxygen evolution reaction: A heteroatom modulator approach. Angew Chem Int Ed, 2020, 59: 16013–16022
165 Yang Y, Qian Y, Li H, *et al.* O-coordinated W-Mo dual-atom catalyst for pH-universal electrocatalytic hydrogen evolution. Sci Adv, 2020, 6: eaba6586
166 Fu J, Yang Y, Hu JS. Dual-sites tandem catalysts for C–N bond formation *via* electrocatalytic coupling of CO_2 and nitrogenous small molecules. ACS Mater Lett, 2021, 3: 1468–1476
167 Ying Y, Luo X, Qiao J, *et al.* "More is different": Synergistic effect and structural engineering in double-atom catalysts. Adv Funct Mater, 2020, 31: 2007423
168 Janssens E, Neukermans S, Wang X, *et al.* Stability patterns of transition metal doped silver clusters: Dopant- and size-dependent electron delocalization. Eur Phys J D, 2005, 34: 23–27
169 Shi ZZ, Li WP, Kang WJ, *et al.* Silver clusters with adatoms as a catalyst for the oxygen reduction reaction. ACS Catal, 2023, 13: 9181–9189
170 Xu W, Wang Y, Zhang C, *et al.* Insights into the electronic structure coupling effect of dual-metal atomic electrocatalytic platform for efficient clean energy conversion. Chem Eng J, 2023, 461: 141911
171 Gong YN, Cao CY, Shi WJ, *et al.* Modulating the electronic structures of dual-atom catalysts *via* coordination environment engineering for boosting CO_2 electroreduction. Angew Chem Int Ed, 2022, 61: e202215187
172 Hao J, Zhuang Z, Hao J, *et al.* Interatomic electronegativity offset dictates selectivity when catalyzing the CO_2 reduction reaction. Adv Energy Mater, 2022, 12: 2200579
173 Zhang J, Huang Q, Wang J, *et al.* Supported dual-atom catalysts: Preparation, characterization, and potential applications. Chin J Catal, 2020, 41: 783–798
174 Wang J, Zhao CX, Liu JN, *et al.* Dual-atom catalysts for oxygen electrocatalysis. Nano Energy, 2022, 104: 107927
175 Hao Q, Zhong H, Wang J, *et al.* Nickel dual-atom sites for electrochemical carbon dioxide reduction. Nat Synth, 2022, 1: 719–728
176 Jiang M, Wang F, Yang F, *et al.* Rationalization on high-loading iron and cobalt dual metal single atoms and mechanistic insight into the oxygen reduction reaction. Nano Energy, 2022, 93: 106793
177 Lv P, Lv W, Wu D, *et al.* Ultrahigh-density double-atom catalyst with spin moment as an activity descriptor for the oxygen-reduction reaction. Phys Rev Appl, 2023, 19: 054094
178 Liu M, Li N, Cao S, *et al.* A "pre-constrained metal twins" strategy to prepare efficient dual-metal-atom catalysts for cooperative oxygen electrocatalysis. Adv Mater, 2022, 34: 2107421
179 Fu J, Dong J, Si R, *et al.* Synergistic effects for enhanced catalysis in a dual single-atom catalyst. ACS Catal, 2021, 11: 1952–1961
180 Yu B, Cheng L, Dai S, *et al.* Silver and copper dual single atoms boosting direct oxidation of methane to methanol *via* synergistic catalysis. Adv Sci, 2023, 10: 2302143
181 Zhang WD, Zhou L, Shi YX, *et al.* Dual-atom catalysts derived from a preorganized covalent organic framework for enhanced electrochemical oxygen reduction. Angew Chem Int Ed, 2023, 62: e202304412

182 Wang Q, Zhou D, Liu C, *et al.* Enhancing effect of dual-atom catalysts on tetrabromobisphenol S degradation *via* peroxydisulfate activation: Synergism of Fe–Cu and electron-transfer mechanism. Chem Eng J, 2023, 460: 140681
183 Yin P, Luo X, Ma Y, *et al.* Sulfur stabilizing metal nanoclusters on carbon at high temperatures. Nat Commun, 2021, 12: 3135
184 Takahashi M, Koizumi H, Chun WJ, *et al.* Finely controlled multimetallic nanocluster catalysts for solvent-free aerobic oxidation of hydrocarbons. Sci Adv, 2017, 3: e1700101
185 Chen X, Peng M, Cai X, *et al.* Regulating coordination number in atomically dispersed Pt species on defect-rich graphene for n-butane dehydrogenation reaction. Nat Commun, 2021, 12: 2664
186 Rong H, Ji S, Zhang J, *et al.* Synthetic strategies of supported atomic clusters for heterogeneous catalysis. Nat Commun, 2020, 11: 5884
187 Wan W, Zhao Y, Wei S, *et al.* Mechanistic insight into the active centers of single/dual-atom Ni/Fe-based oxygen electrocatalysts. Nat Commun, 2021, 12: 5589
188 Li L, Larsen AH, Romero NA, *et al.* Investigation of catalytic finite-size-effects of platinum metal clusters. J Phys Chem Lett, 2012, 4: 222–226
189 Liu J, Krishna KS, Losovyj YB, *et al.* Ligand-stabilized and atomically precise gold nanocluster catalysis: A case study for correlating fundamental electronic properties with catalysis. Chem Eur J, 2013, 19: 10201–10208
190 Li H, Li L, Li Y. The electronic structure and geometric structure of nanoclusters as catalytic active sites. Nanotechnol Rev, 2013, 2: 515–528
191 Li M, Cui Y, Zhang X, *et al.* Screening a suitable Mo form supported on graphdiyne for effectively electrocatalytic N_2 reduction reaction: From atomic catalyst to cluster catalyst. J Phys Chem Lett, 2020, 11: 8128–8137
192 Vorobyeva E, Fako E, Chen Z, *et al.* Atom-by-atom resolution of structure-function relations over low-nuclearity metal catalysts. Angew Chem Int Ed, 2019, 58: 8724–8729
193 Ji S, Chen Y, Fu Q, *et al.* Confined pyrolysis within metal-organic frameworks to form uniform Ru_3 clusters for efficient oxidation of alcohols. J Am Chem Soc, 2017, 139: 9795–9798
194 Imaoka T, Kitazawa H, Chun WJ, *et al.* Magic number Pt_{13} and misshapen Pt_{12} clusters: Which one is the better catalyst? J Am Chem Soc, 2013, 135: 13089–13095
195 Gu J, Xu Y, Lu J. Atom-precise low-nuclearity cluster catalysis: Opportunities and challenges. ACS Catal, 2023, 13: 5609–5634
196 Tyo EC, Vajda S. Catalysis by clusters with precise numbers of atoms. Nat Nanotech, 2015, 10: 577–588
197 Chakraborty I, Pradeep T. Atomically precise clusters of noble metals: Emerging link between atoms and nanoparticles. Chem Rev, 2017, 117: 8208–8271
198 Niihori Y, Matsuzaki M, Pradeep T, *et al.* Separation of precise compositions of noble metal clusters protected with mixed ligands. J Am Chem Soc, 2013, 135: 4946–4949
199 Sun G, Alexandrova AN, Sautet P. Structural rearrangements of subnanometer Cu oxide clusters govern catalytic oxidation. ACS Catal, 2020, 10: 5309–5317
200 Kaden WE, Wu T, Kunkel WA, *et al.* Electronic structure controls reactivity of size-selected Pd clusters adsorbed on TiO_2 surfaces. Science, 2009, 326: 826–829
201 Raja R, Hermans S, Shephard DS, *et al.* Preparation and characterisation of a highly active bimetallic (Pd–Ru) nanoparticle heterogeneous catalyst. Chem Commun, 1999, 10.1039/a901263j: 1571–1572
202 Mitchell S, Pérez-Ramírez J. Atomically precise control in the design of low-nuclearity supported metal catalysts. Nat Rev Mater, 2021, 6: 969–985
203 Giulimondi V, Kaiser SK, Agrachev M, *et al.* Redispersion strategy for high-loading carbon-supported metal catalysts with controlled nuclearity. J Mater Chem A, 2022, 10: 5953–5961
204 Yan G, Tang Y, Li Y, *et al.* Reaction product-driven restructuring and assisted stabilization of a highly dispersed Rh-on-ceria catalyst. Nat Catal, 2022, 5: 119–127
205 Lei Y, Mehmood F, Lee S, *et al.* Increased silver activity for direct propylene epoxidation *via* subnanometer size effects. Science, 2010, 328: 224–228
206 Li X, Mitchell S, Fang Y, *et al.* Advances in heterogeneous single-cluster catalysis. Nat Rev Chem, 2023, 7: 754–767
207 Lu Y, Chen W. Sub-nanometre sized metal clusters: From synthetic challenges to the unique property discoveries. Chem Soc Rev, 2012, 41: 3594–3623
208 Huang JF, Zeng RH, Chen JL. Thermostable carbon-supported sub-nanometer-sized (<1 nm) Pt clusters for the hydrogen evolution reaction. J Mater Chem A, 2021, 9: 21972–21980
209 Compton AH. The size and shape of the electron. Phys Rev, 1919, 14: 247–259
210 Francke R, Little RD. Electrons and holes as catalysts in organic electrosynthesis. ChemElectroChem, 2019, 6: 4373–4382
211 Jiao Y, Qiu Y, Zhang L, *et al.* Electron-catalysed molecular recognition. Nature, 2022, 603: 265–270
212 Broese T, Roesel AF, Prudlik A, *et al.* An electrocatalytic Newman–Kwart-type rearrangement. Org Lett, 2018, 20: 7483–7487
213 Qi Y, Li J, Zhang Y, *et al.* Novel lignin-based single atom catalysts as peroxymonosulfate activator for pollutants degradation: Role of single cobalt and electron transfer pathway. Appl Catal B-Environ, 2021, 286: 119910
214 Wu H, Yan J, Xu X, *et al.* Synergistic effects for boosted persulfate activation in a designed Fe–Cu dual-atom site catalyst. Chem Eng J, 2022, 428: 132611
215 Wang Y, Yin H, Dong F, *et al.* N-coordinated Cu-Ni dual-single-atom catalyst for highly selective electrocatalytic reduction of nitrate to ammonia. Small, 2023, 19: 2207695
216 Mallick K, Witcomb M, Scurrell M. Silver nanoparticle catalysed redox reaction: An electron relay effect. Mater Chem Phys, 2006, 97: 283–287
217 Ma M, Guo S, Sang X, *et al.* Structure, synthesis, and properties of single-metal-atom chains. Cell Rep Phys Sci, 2022, 3: 101124
218 Chen Y, He T, Liu Q, *et al.* Highly durable iron single-atom catalysts for low-temperature zinc-air batteries by electronic regulation of adjacent iron nanoclusters. Appl Catal B-Environ, 2023, 323: 122163
219 Li X, Pereira-Hernández XI, Chen Y, *et al.* Functional CeO_x nanoglues for robust atomically dispersed catalysts. Nature, 2022, 611: 284–288
220 Lang R, Xi W, Liu JC, *et al.* Non defect-stabilized thermally stable single-atom catalyst. Nat Commun, 2019, 10: 234
221 Joo SH, Park JY, Tsung CK, *et al.* Thermally stable Pt/mesoporous silica core–shell nanocatalysts for high-temperature reactions. Nat Mater, 2008, 8: 126–131
222 Dai Y, Lim B, Yang Y, *et al.* A sinter-resistant catalytic system based on platinum nanoparticles supported on TiO_2 nanofibers and covered by porous silica. Angew Chem Int Ed, 2010, 49: 8165–8168
223 Liang XM, Wang HJ, Zhang C, *et al.* Controlled synthesis of a Ni_2 dual-atom catalyst for synergistic CO_2 electroreduction. Appl Catal B-Environ, 2023, 322: 122073
224 Duan S, Wang R, Liu J. Stability investigation of a high number density Pt_1/Fe_2O_3 single-atom catalyst under different gas environments by HAADF-STEM. Nanotechnology, 2018, 29: 204002
225 Liu L, Díaz U, Arenal R, *et al.* Generation of subnanometric platinum with high stability during transformation of a 2D zeolite into 3D. Nat Mater, 2016, 16: 132–138
226 Qian M, Wu XL, Lu M, *et al.* Modulation of charge trapping by island-like single-atom cobalt catalyst for enhanced photo-fenton-like reaction. Adv Funct Mater, 2023, 33: 2208688
227 Jiang W, Zhu H, Yang J, *et al.* Integration of single-atom catalyst with Z-scheme heterojunction for cascade charge transfer enabling highly efficient piezo-photocatalysis. Adv Sci, 2023, 10: 2303448
228 Li W, Liu C, Gu C, *et al.* Interlayer charge transfer regulates single-atom catalytic activity on electride/graphene 2D heterojunctions. J Am Chem Soc, 2023, 145: 4774–4783
229 Zhang Y, Johannessen B, Zhang P, *et al.* Reversed electron transfer in dual single atom catalyst for boosted photoreduction of CO_2. Adv Mater, 2023, 35: 2306923
230 Feng K, Zhang H, Gao J, *et al.* Single atoms or not? The limitation of EXAFS. Appl Phys Lett, 2020, 116: 191903

Acknowledgements This work was supported by the National Natural Science Foundation of China (52172046).

Author contributions Wang H wrote the paper; Li J revised the manuscript; Zhu H provided the overall concept and revised the manuscript. All authors participated in the discussion.

Conflict of interest The authors declare that they have no conflict of interest.

Honglin Wang is a PhD candidate at the School of Materials Science and Engineering, Tsinghua University. She received her BS degree from Tsinghua University in 2022. Her research interests focus on 2D materials and SACs.

Hongwei Zhu is a professor at the School of Materials Science and Engineering, Tsinghua University. He received his BS degree in mechanical engineering (1998) and PhD degree in materials processing engineering (2003) from Tsinghua University. After Post Doc. studies in Japan and the USA, he began his independent career as a faculty member at Tsinghua University (2008–present). His current research interests involve low-dimensional materials and materials informatics.

催化中的极限结构: 单原子, 亚纳米团簇和电子

王泓麟[1], 李晶[2], 朱宏伟[1*]

摘要 催化剂的尺寸在降低到原子尺度时表现出显著的性能提升, 如原子利用率提高、配位不饱和度增强和比表面积增加. 为了实现高效催化, 针对原子分布和电子行为的精细设计与调控至关重要, 由此引入了“极限结构”这一概念. 极限结构涵盖了单个原子、双原子, 单个原子链/层和亚纳米团簇等结构. 围绕这些极限结构在原子和电子尺度上研究催化剂, 可以更深入地理解其本征性质并为未来的催化剂设计提供新的方向. 本文总结了极限结构在催化应用中的最新进展和研究方向, 重点讨论单原子、亚纳米团簇和电子尺度的反应动力学. 特别关注极限结构的优化策略, 如金属-支撑作用增强、缺陷和电子结构调控. 探讨了各种极限结构之间的相互关系, 强调了每个结构的特性. 最后, 展望了极限结构在催化领域的未来发展趋势.

